NUREG/CR-5534
PSU/ME-98-7321

Critical Heat Flux (CHF) Phenomenon on a Downward Facing Curved Surface: Effects of Thermal Insulation

Prepared by
F. B. Cheung, Y. C. Liu

The Pennsylvania State University

Prepared for
U.S. Nuclear Regulatory Commission

0/1

DF02

AVAILABILITY NOTICE

Availability of Reference Materials Cited in NRC Publications

NRC publications in the NUREG series, NRC regulations, and *Title 10, Energy*, of the *Code of Federal Regulations*, may be purchased from one of the following sources:

1. The Superintendent of Documents
   U.S. Government Printing Office
   P.O. Box 37082
   Washington, DC 20402–9328
   <http://www.access.gpo.gov/su_docs>
   202–512–1800

2. The National Technical Information Service
   Springfield, VA 22161–0002
   <http://www.ntis.gov/ordernow>
   703–487–4650

The NUREG series comprises (1) technical and administrative reports, including those prepared for international agreements, (2) brochures, (3) proceedings of conferences and workshops, (4) adjudications and other issuances of the Commission and Atomic Safety and Licensing Boards, and (5) books.

A single copy of each NRC draft report is available free, to the extent of supply, upon written request as follows:

Address: Office of the Chief Information Officer
Reproduction and Distribution
Services Section
U.S. Nuclear Regulatory Commission
Washington, DC 20555–0001
E–mail: <GRW1@NRC.GOV>
Facsimile: 301–415–2289

A portion of NRC regulatory and technical information is available at NRC's World Wide Web site:

<http://www.nrc.gov>

All NRC documents released to the public are available for inspection or copying for a fee, in paper, microfiche, or, in some cases, diskette, from the Public Document Room (PDR):

NRC Public Document Room
2121 L Street, N.W., Lower Level
Washington, DC 20555–0001
<http://www.nrc.gov/NRC/PDR/pdr1.htm>
1–800–397–4209 or locally 202–634–3273

Microfiche of most NRC documents made publicly available since January 1981 may be found in the Local Public Document Rooms (LPDRs) located in the vicinity of nuclear power plants. The locations of the LPDRs may be obtained from the PDR (see previous paragraph) or through:

<http://www.nrc.gov/NRC/NUREGS/SR1350/V9/lpdr/html>

Publicly released documents include, to name a few, NUREG-series reports; *Federal Register* notices; applicant, licensee, and vendor documents and correspondence; NRC correspondence and internal memoranda; bulletins and information notices; inspection and investigation reports; licensee event reports; and Commission papers and their attachments.

Documents available from public and special technical libraries include all open literature items, such as books, journal articles, and transactions, *Federal Register* notices, Federal and State legislation, and congressional reports. Such documents as theses, dissertations, foreign reports and translations, and non-NRC conference proceedings may be purchased from their sponsoring organization.

Copies of industry codes and standards used in a substantive manner in the NRC regulatory process are maintained at the NRC Library, Two White Flint North, 11545 Rockville Pike, Rockville, MD 20852–2738. These standards are available in the library for reference use by the public. Codes and standards are usually copyrighted and may be purchased from the originating organization or, if they are American National Standards, from—

American National Standards Institute
11 West 42nd Street
New York, NY 10036–8002
<http://www.ansi.org>
212–642–4900

NUREG/CR-5534
PSU/ME-98-7321

Critical Heat Flux (CHF) Phenomenon on a Downward Facing Curved Surface: Effects of Thermal Insulation

Manuscript Completed: August 1998
Date Published: September 1998

Prepared by
F. B. Cheung, Y. C. Liu

Department of Mechnical Engineering
The Pennsylvania State University
University Park, PA 16802-1412

A. Behbahani, NRC Project Manager

Prepared for
Division of Systems Technology
Office of Nuclear Regulatory Research
U.S. Nuclear Regulatory Commission
Washington, DC 20555-0001
NRC Job Code J6030

ABSTRACT

The phenomena of natural convection boiling and critical heat flux on the outer surface of a heated hemispherical vessel surrounded by a thermal insulation structure were investigated experimentally in the subscale boundary layer boiling (SBLB) test facility. The objectives were to measure the rate of boiling heat transfer, to observe the behavior of the boiling-induced two-phase motion in the annular channel formed between the hemispherical vessel and the insulation structure, and to determine the flow effect on the critical heat flux on the downward-facing hemispherical surface. High-speed photographic records revealed the presence of violent cyclic ejection of the vapor masses generated by boiling on the vessel outer surface which resulted in a buoyancy-driven, upward, co-current two-phase flow through the channel. A one-dimensional analysis of the co-current flow in the channel indicated that the induced mass flow rate was a strong function of the wall heat flux and the size of the channel. Measurements of the local boiling heat fluxes and the local wall superheats showed a significant spatial variation of the nucleate boiling heat transfer, evidently due to the effect of the upward co-current flow. At high heat flux levels, the steam venting process through the minimum gap of the channel was found to be highly unsteady and chaotic. Owing to the chaotic steam venting process, the local critical heat flux had the lowest value near the minimum gap. However, this lowest value is still higher than the corresponding local CHF value for the case without thermal insulation.

CONTENTS

Page

Abstract iii

Executive Summary ix

1. Introduction 1

   1.1 Background 1

   1.2 Major Objectives 3

   1.3 References 4

2. Experimental Methods 5

   2.1 Test Apparatus 5

   2.2 Experimental Procedure 6

   2.3 Measurement Techniques 9

   2.4 References 10

3. Analysis of the Upward Co-Current Flow Induced by the Natural Convection Boiling Process 11

   3.1 The Continuity Equation 11

   3.2 The Momentum Equation for One-Dimensional Two-Phase Flow 11

   3.3 The Energy Equation for One-Dimensional Two-Phase Flow 13

   3.4 Two-Phase Frictional Pressure Drop 14

   3.5 Other Pressure Drops 15

   3.6 Numerical Solution Scheme 15

   3.7 References 17

   3.8 Nomenclature 17

4. Results and Discussion 19

4.1 Vapor Dynamics and Two-Phase Flow Phenomenon 19

4.2 Numerical Prediction of the Upward Co-Current Flow 20

4.3 Natural Convection Boiling Heat Transfer 21

4.4 Spatial Variation of the Critical Heat Flux 27

4.5 References 31

5. Conclusions 33

Appendices

Appendix A Literature Survey A-1

Appendix B Program Listing for Flow Calculations B-1

Appendix C Steady-State Nucleate Boiling Data for a Downward Facing Hemispherical Surface Surrounded by a Thermal Insulation Structure C-1

Figures

Figure 1.1 Schematic of the Reactor Vessel in a Flooded Cavity Surrounded by a Thermal Insulation Structure 2

Figure 2.1 Dimensions of the Water Tank with a Condenser Unit Employed in the Experiment 7

Figure 2.2 Schematic of the Simulated Reactor Vessel Surrounded by a Scaled Insulation Structure in the Water Tank 7

Figure 2.3 Top View of the Scaled Thermal Insulation Structure Showing the Connection between the Upper Cylindrical and the Lower Octagonal Parts 8

Figure 2.4 Side View of the Scaled Thermal Insulation Structure Showing the Two Sets of Horizontal Slots for Venting of Water and Steam 8

Figure 2.5 Schematic of the Power Control System Used to Detect the Occurrence of CHF on the Vessel Wall 10

Figure 3.1 Schematic of the Important Flow Quantities in the Flow Channel Considered in the One-Dimensional Analysis 12

Figure 3.2 Schematic of the Annular Channel Formed Between the Scaled Reactor Vessel and the Thermal Insulation Structure. 12

Figure 3.3 Flow Chart for Calculating the Mass Flow Rate from the Momentum Equation 16

Figure 4.1 The Predicted Total Mass Flow Rate in the Annular Channel as a Function of the Heat Flux Level and the Channel Size 22

Figure 4.2 Spatial Variation of the Local Vapor Flow Rate Along the Vessel Outer Surface at Various Heat Flux Levels 22

Figure 4.3 Spatial Variation of the Local Liquid Flow Rate Along the Vessel Outer Surface at Various Heat Flux Levels 23

Figure 4.4 Spatial Variation of the Local Void Fraction in the Annular Channel at Various Heat Flux Levels 23

Figure 4.5 Spatial Variation of the Superficial Vapor Velocity Along the Vessel Outer Surface at Various Heat Flux Levels 24

Figure 4.6 Natural Convection Boiling Data at the External Bottom Center ($\theta = 0°$) 24

Figure 4.7 Natural Convection Boiling Data at an Off-Center Location ($\theta = 18°$) 25

Figure 4.8 Natural Convection Boiling Data at an Off-Center Location ($\theta = 45°$) 25

Figure 4.9 Natural Convection Boiling Data at an Off-Center Location ($\theta = 60°$) 26

Figure 4.10 Natural Convection Boiling Data at an Off-Center Location ($\theta = 75°$) 26

Figure 4.11 Spatial Variation of the Natural Convection Boiling Data Under Saturated Boiling Conditions ($T_{water} = 100°C$) 28

Figure 4.12 Spatial Variation of the Natural Convection Boiling Data Under Subcooled Boiling Conditions ($T_{water} = 97°C$) 28

Figure 4.13 Spatial Variation of the Natural Convection Boiling Data Under Subcooled Boiling Conditions ($T_{water} = 93°C$) 29

Figure 4.14 Spatial Variation of the Natural Convection Boiling Data Under Subcooled Boiling Conditions ($T_{water} = 90°C$) 29

Figure A.1 Schematic Representations of Postulated CHF Mechanisms A-1

Figure A.2 Pool Boiling on Curved Surface A-9

Figure A.3 Idealized Model System Used in the Analysis of Annular Flow Without Entrainment A-14

Tables

Table 4.1 Local Critical Heat Flux (CHF) for the Cases With and Without Thermal Insulation 30

Table A.1 Effects of Subcooling and Gap Size on the CHF Limit-Comparison of Previous Studies A-7

Table A.2 The CHF Mechanism Under Various Mass Flux and Subcooling Conditions Comparison of Previous Studies A-8

Table A.3 Critical Heat Flux Values Reported by Previous Investigators A-10

Table A.4 Constants Used in the Lockhart and Martinelli Correlation A-16

Table A.5 Constants Used in Various Correlations for Void Fraction A-17

EXECUTIVE SUMMARY

The Phenomena of natural convection boiling and critical heat flux on the outer surface of a heated hemispherical vessel surrounded by a thermal insulation structure were investigated experimentally in the Subscale Boundary Layer Boiling (SBLB) Test Facility at Penn State. The objectives were to measure the rate of boiling heat transfer, to observe the behavior of the boiling-induced two-phase motions in the annular channel formed between the hemispherical vessel and the insulation structure, and to determine the flow effect on the local critical heat flux on the vessel outer surface. The test vessel, having a diameter of 12" (0.305m), consisted of a cylindrical upper part and a hemispherical lower part. The thermal insulation structure, made of transparent material to allow direct flow observations, had a cylindrical upper part and an octagonal lower part that formed an annular channel with the test vessel. Heat transfer measurements at various angular positions of the test vessel were made under both saturated and subcooled boiling conditions along with observations of the boiling-induced two-phase motions in the annular channel.

High-speed photographic studies were performed to seek a clear physical understanding of the vapor dynamics and the two-phase flow through the annular channel under steady-state boiling conditions. The photographic records revealed the presence of violent cyclic ejection of large elongated vapor masses generated by boiling on the vessel outer surface, which resulted in a buoyancy-driven upward co-current two-phase flow through the channel. At high-heat-flux levels, the steam venting process through the minimum gap of the channel was found to be highly unsteady and chaotic. Strong upstream influences were observed as a result of the activities of large elongated bubbles that were generated in the bottom center region of the vessel. Because of the upward co-current flow, water was being entrained at a significant rate from the bottom of the channel. Thus, a much higher two-phase flow rate was induced on the vessel outer surface in the present case compared to the case without thermal insulation.

To complement the experimental effort, a one-dimensional two-phase flow analysis was performed to predict the mass flow rate of the upward co-current two-phase flow that would be induced in the annular channel at various heat flux levels. The momentum equation was integrated numerically using an iterative scheme based on the Secant method to calculate the induced mass flow rate and the two-phase pressure drop. The numerical results indicated that the mass flow rate of the upward co-current flow in the annular channel was a strong function of the wall heat flux and the size of the channel (gap and height). For wall heat fluxes less then ~ $0.7MW/m^2$, the mass flow rate increased as the wall heat flux was increased. On the other head, for wall heat fluxes larger than ~ $0.7MW/m^2$, the reverse was found to be the case. At a given heat flux level, the mass flow rate tended to decrease as the channel gap was decreased, apparently due to the increase in the two-phase pressure drop.

Measurements of the local boiling heat transfer were made under steady-state boiling conditions at high-heat-flux levels. The local critical heat fluxes at various positions of the vessel outer surface were found to be much higher than the corresponding local CHF values for the case

without thermal insulation. This enhancement in the local critical heat flux was evidently a result of the increased flow entrainment in the channel for the case with thermal insulation. In addition to the magnitude of the local critical heat flux, the presence of thermal insulation also affected the spatial variation of the critical heat flux. With thermal insulation, the local CHF no longer increased monotonically along the vessel outer surface. Rather, it exhibited a minimum near the minimum gap, evidently due to the unsteady and chaotic steam venting process through the gap.

1. INTRODUCTION

1.1 Background

In the event of an inadequate core cooling in an advanced light water reactor (ALWR), a significant amount of core material can become molten and relocate downward into the lower head of the reactor pressure vessel (RPV). To maintain the integrity of the lower head, it is essential that the decay heat transferred downward from the core melt to the vessel wall be effectively removed from the vessel outer surface to a permanent heat sink. One viable means of doing that is to make water available on the external bottom side of the RPV by flooding the reactor cavity under severe accident conditions. Design features of most ALWRs have the provision for substantial water accumulation within the containment during numerous postulated accident sequences. With the water covering the external surfaces of the lower head, significant energy (i.e., decay heat) could be removed from the core melt through the vessel wall by nucleate boiling on the vessel outer surface. As long as the wall heat flux from the core melt would not exceed the critical heat flux (CHF) limit for nucleate boiling on the vessel outer surface, the reactor vessel could be sufficiently cooled so as to prevent downward failure of the vessel and release of the core melt into the containment.

In an attempt to evaluate the concept of external vessel cooling by cavity flooding, a subscale boundary layer boiling (SBLB) test facility was developed at Penn State with the aid of a scaling analysis to simulate the phenomena of pool boiling and critical heat flux (CHF) on the external bottom surface of a heated hemispherical vessel. Saturated and subcooled boiling experiments were performed in the SBLB facility to measure the spatial variation of the critical heat flux and observe the underlying mechanisms, including the vapor dynamics and the resulting buoyancy-driven, external, two-phase boundary layer flow along the downward-facing hemispherical heating surface for the case without thermal insulation [1]. Based on the experimental evidence and an advanced hydrodynamic CHF model [2], a scaling law was established for estimating the local critical heat flux on the vessel outer surface. The scaling law, which compared favorably with the available CHF data obtained for various vessel sizes, was shown to be capable of predicting the local CHF limits on large commercial-size vessels for the case without thermal insulation [1].

In many ALWR designs, the reactor vessel is surrounded by a thermal insulation structure as shown schematically in Figure 1.1. The insulation structure, having a cylindrical upper part and an octagonal lower part, forms a hemispherical annular channel with the reactor vessel. A small flow inlet is made available at the bottom center of the insulation structure to allow water to enter the annular channel. As boiling of the water takes place on the vessel outer surface under severe accident conditions, the vapor masses generated on the downward-facing hemispherical heating surface tend to flow upward through the channel under the influence of gravity. Because of the vapor motion, liquid water is entrained in the flow, thus resulting in an upward co-current two-phase motion in the channel. While the flow is induced entirely by the boiling process, the rate of boiling on the downward-facing hemispherical surface, in turn, can be significantly affected by the resulting two-phase motion. Thus far, this unconventional natural convection boiling process has not

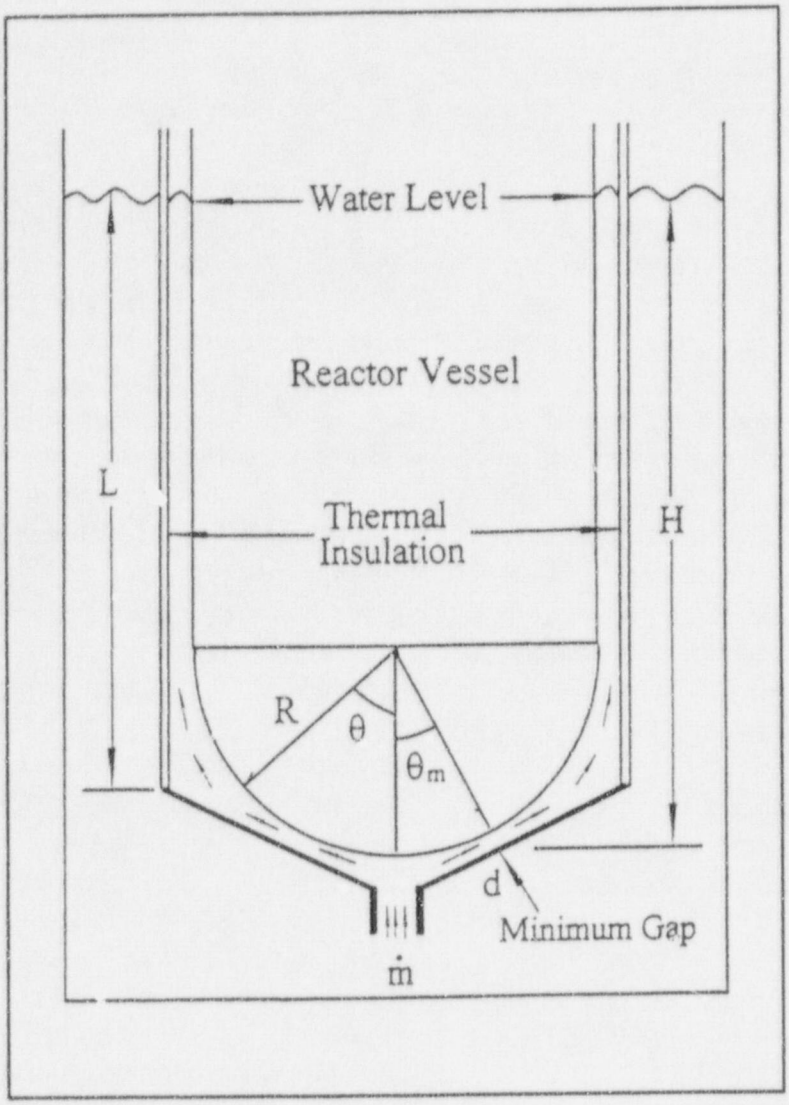

Figure 1.1 Schematic of the Reactor Vessel in a Flooded Cavity Surrounded by a Thermal Insulation Structure.

been seriously investigated by previous researchers.

Most studies of natural convection boiling have been restricted to those processes taking place in narrow or confined spaces [3]. Ishibashi and Nishikawa [4] identified the isolated bubble region and the coalesced bubble region for nucleate boiling in the low-heat-flux regime in a vertical annuli of a heated core and unheated external shroud with both ends open. Vishnev et al. [5] measured the critical heat flux in vertical channels with natural convection. Katto and his co-workers [6-8] developed generalized correlations for the critical heat flux of natural convection boiling in confined spaces, vertical annular channels, and uniformly heated vertical round tubes. Monde et al. [9] obtained a correlation for

the critical heat flux of natural convection boiling in vertical rectangular channels submerged in saturated liquids heated on one side. Yao and Chang [10] studied natural convection boiling in a vertical annuli with a closed bottom and identified three boiling regimes of isolated deformed bubbles, slightly deformed bubbles, and coalesced deformed bubbles. Fujita et al. [11] and Fujita and Uchida [12] measured the nucleate boiling heat transfer and critical heat flux for natural convection boiling in thin vertical rectangular channels and in a confined narrow space, respectively. Most recently, Asmolov et al. [13] performed gap-boiling experiments to measure the nucleate boiling heat transfer and critical heat flux for natural convection boiling in a vertical flat channel formed by two parallel plates that were heated either on both sides or on one side only. A comprehensive review of the literature is presented in Appendix A.

As can be seen in Appendix A, none of the previous studies is applicable to the problem under consideration. This is because of the differences in the size of the channel and the geometry of the heating surface between the previous studies and the present work. Both factors (i.e., the size and the geometry) are expected to have strong effects on the natural convection boiling process. The channel sizes employed in most previous studies were at least an order of magnitude smaller than the size of the hemispherical flow channel considered in the present work. Moreover, the heating surface employed in this study is a downward facing curved surface, as shown in Figure 1.1. This geometry is significantly different than those used by previous investigators which were vertical or inclined flat surfaces. Because of the relatively large channel size and the downward orientation of the heating surface employed in this study, the natural convection boiling phenomenon can be quite different than those reported before.

1.2 Major Objectives

In this project, a scaled thermal insulation structure is employed in the existing SBLB test facility to form an annular channel with the hemispherical test vessel depicted in Figure 1.1. Steady state boiling experiments are performed under both saturated and subcooled conditions to observe the vapor dynamics on the vessel outer surface and the boiling-induced two-phase flow behavior in the annular channel. Quantitative measurements are made to determine the flow effects on the natural convection boiling heat transfer and the local critical heat flux on the downward facing hemispherical heating surface. Special attention is given to the steam venting process through the minimum gap of the channel at high heat flux levels, especially when the condition of CHF is approached. The major objectives are:

- To simulate the natural convection boiling process and the phenomenon of critical heat flux on the vessel outer surface surrounded by the thermal insulation structure.

- To observe the boiling events under high-heat-flux conditions and to study the resulting two-phase motions in the annular channel formed between the vessel and the insulation structure.

- To seek a clear physical understanding of the vapor dynamics on the heating surface and the buoyancy-driven two-phase flow behavior in the channel under high-heat-flux boiling conditions.

- To perform a quantitative measurement of the local boiling heat fluxes and the local wall superheats at various positions of the vessel and for different degrees of subcooling.

- To determine the effect of thermal insulation on the spatial variation of the critical heat flux by comparing the data for the cases with and without thermal insulation.

The above objectives are met by performing flow observations as well as heat transfer measurements in the SBLB test facility.

1.3 References

1. Cheung, F. B., K. H. Haddad, and Y. C. Liu, "Critical Heat Flux (CHF) Phenomenon on a Downward Facing Curved Surface," NUREG/CR-6507, U. S. Nuclear Regulatory Commission, Washington, D. C., 1997.

2. Cheung, F. B., and K. H. Haddad, "A Hydrodynamic Critical Heat Flux Model for Saturated Pool Boiling on a Downward Facing Curved Heating Surface, "*Int. J. Heat Mass Transfer*, Vol. 40, No. 6, PP. 1291-1302, 1997.

3. Carey, V., "Liquid-Vapor Phase-Change Phenomena," Hemisphere Publishing Corp., New York, 1992.

4. Ishibashi, E. and K. Nishikawa, "Saturated Boiling Heat Transfer in Narrow Spaces," *Int. J. Heat Mass Transfer*, Vol. 12, PP. 863-894, 1969.

5. Vishnev, I. P., et al., "Nucleate Boiling in Crisis of Helium in Vertical Channels with Natural Convection," *Heat Transfer Soviet Research*, Vol. 6, PP. 170-176, 1974.

6. Katto, Y., "Generalized Correlation for Critical Heat Flux of Natural Convection Boiling in Confined Channels," *Transaction of JSME*, Vol. 44, PP. 3908-3911, 1978.

7. Katto, Y. and T. Kurosaka, "Critical Heat Flux of Natural Convection Boiling in Vertical Annular Channels," *15th National Heat Transfer Symposium of Japan*, PP. 280-282, 1979.

8. Kawamura, S. and Y. Katto, Critical Heat Flux of Natural Convection Boiling in Vertical Uniform Heated Round Tubes," *16th National Heat Transfer Symposium of Japan*, PP. 280-282, 1980.

9. Monde, M., H. Kusuda, and H. Vehera, "Critical Heat Flux During Natural Convection Boiling in Vertical Rectangular Channels Submerged in Saturated Liquid," *J. Heat Transfer*, Vol. 104, PP. 300-303, 1982.

10. Yao, S. C. and Y. Chang, "Pool Boiling Heat Transfer in a Confined Space," *Int. J. Heat Mass Transfer*, Vol. 26, PP. 841-848, 1983.

11. Fujita, Y., H. Ohta, S. Uchida and K. Nishikawa, "Nucleate Boiling Heat Transfer and Critical Heat Flux in Narrow Space Between Rectangular Surfaces," *Int. J. Heat Mass Transfer*, Vol. 31, PP. 229-239, 1988.

12. Fujita, Y. and S. Uchida, "Boiling Heat Transfer and Critical Heat Flux in a Confined Narrow Space," *Proc. Nineth Int. Heat Transfer Conf.*, Hemisphere Publishing Corp, New York, 1990.

13. Asmolov, V. L., L. Kobzar, V. Nikulshin and V. Strizkov, "Experimental Investigation of Critical Heat Flux in Gaps," Cooperative Severe Accident Research Program (CSARP) Meeting, Bethesda, Maryland, 1997.

2. EXPERIMENTAL METHOD

The effects of thermal insulation on the natural convection boiling process and the CHF phenomenon on the outer surface of a hemispherical vessel surrounded by a thermal insulation structure were investigated in the SBLB test facility. A detailed description of the various components of the test facility for the case without thermal insulation was given in [1]. In the present project, the experimental setup was essentially the same as the one described in [1]. The only difference was the installation of two additional components, one being a scaled cylinder connected to the hemispherical test vessel to simulate the upper cylindrical part of an advanced reactor vessel and the other being a scaled insulation structure that formed an annular flow channel with the vessel. A brief description of the test apparatus, the experimental procedure, and the measurement techniques are given below.

2.1 Test Apparatus

The experimental apparatus consisted of a water tank with a condenser unit, a test vessel with a scaled thermal insulation structure, a data acquisition and photographic system, and a power control system. The water tank was made of carbon steel and had dimensions shown in Figure 2.1. Two large and one small viewing windows were installed on the tank to observe, video-tape, and take high-speed films and instantaneous pictures of the boiling event as well as the resulting two-phase flow configuration. The two large windows were placed on two opposite sides of the tank. One was used for the recording system along with light sources and the other was used for additional lighting as deemed necessary. The small window was used to observe the water level while the tank was being filled with water and to know the exact location of the test vessel inside the tank. Three immersion heaters were installed near the bottom of the tank to preheat the water to a desired temperature before a run. The water tank was completely sealed and could be operated at a system pressure up to 20 psig.

The water level was maintained constant in the tank during a run by using a condenser unit on top of the water tank to condense the vapor masses generated by boiling with the condensate being returned to the bottom of the tank. Owing to the height of the water level, a small temperature gradient could exist in the water tank with the hot liquid accumulating at the top. Three thermocouples were installed along the inside of the tank wall to assess the temperature variation in the water tank. They were inserted inside the tank at the same location shown under item "m" in Figure 2.1. One sensed the water temperature in the middle of the tank, another was bent upward to measure the temperature near the water surface and the third was bent downward to keep track of the water temperature near the bottom of the tank.

The test vessel, made of pure aluminum, had a diameter of 0.3m. It consisted of a heated hemispherical lower part to simulate the lower head of a reactor vessel, and an unheated cylindrical upper part to simulate the upper part of a reactor vessel. The hemispherical lower part of the test vessel was 0.15m in height whereas the cylindrical upper part was 0.7m in height. There were five segments in the lower part, each having the same heat transfer area. Uniformly spaced independent heating elements were installed on the interior side of each segment

to provide a local wall heat flux up to 1.2 MW/m^2. The test vessel was surrounded by a scaled thermal insulation structure (see Figure 2.2) that was fabricated to simulate the hydrodynamic aspects of the thermal insulation system of an advanced light water reactor. The dimensions of the scaled insulation structure were based on a scaling analysis of the actual system [1]. The scaled insulation structure, having a nominal diameter of 0.38m, consisted of an upper cylindrical part and a lower octagonal part (see Figure 2.3). The upper part was approximately 0.72m in height and had two sets of six horizontal opening slots (each having a length of 0.08m) near the top for venting of the water and the steam (see Figure 2.4). The lower part was made up of eight equal-sized panels with a small opening (approximately 0.038m in diameter) at the bottom center for water ingression, as shown in Figure 2.3. Both parts were made up of plexiglas material so that the entire structure was transparent, suitable for direct flow observations.

2.2 Experimental Procedure

To prepare for a run, the hemispherical test vessel was thoroughly cleaned. First the vessel outer surface was polished with #220 emery paper and then it was cleaned with acetone. The test vessel was then connected to the upper cylindrical part and the entire reactor vessel simulator was mounted vertically to the tank access hole cover as shown in Figure 2.2. When the test vessel was properly positioned, the power supply cables and the thermocouple wires were attached to the interior side of the vessel with the other ends connected to the data acquisition system. The viewing windows were sealed and the three thermocouples for measuring the water temperatures in the tank were also connected to the data acquisition system.

The scaled insulation structure was mounted symmetrically to the aluminum test vessel to form a flow annulus. To do this, the upper part of the insulation structure was properly aligned with the center cover plate of the water tank to assure a uniform circumferential gap between the test vessel and the insulation structure. By changing the vertical position of the center cover plate using annular spacers, the height of the insulation structure submerged in the water could be adjusted. In so doing, the size of the minimum gap of the channel (see Figure 1.1) between the octagonal lower part of the insulation structure and the hemispherical lower part of the test vessel could be varied. To facilitate flow observation, a dye-injection apparatus having a multiple injection points near the tip, was positioned right underneath the flow inlet at the bottom center of the octagonal lower part of the insulation structure. The dye injection rate was controlled by a valve with variable settings.

After the vessel and the insulation structure were put in place, a hose was connected to a tap water supply line in order to bring the water level inside the tank to about 0.84m. The hose was equipped with a filter to get rid of any unwanted particles. When the desired water level was attained, the faucet was turned off and the three immersion heaters were turned on. It took about four hours to heat the water to the saturation temperature. At this point, the heaters were kept on for another 15 minutes to degas the water. Then the heaters were turned off to let the water cool back down to room temperature. A pump was then used to circulate the water through the filter again. This helped remove the particles that precipitated during the heating process. The heaters were turned on again to heat the water to the desired temperature. If the temperature fell below the desired value during the experiment, one of the heaters

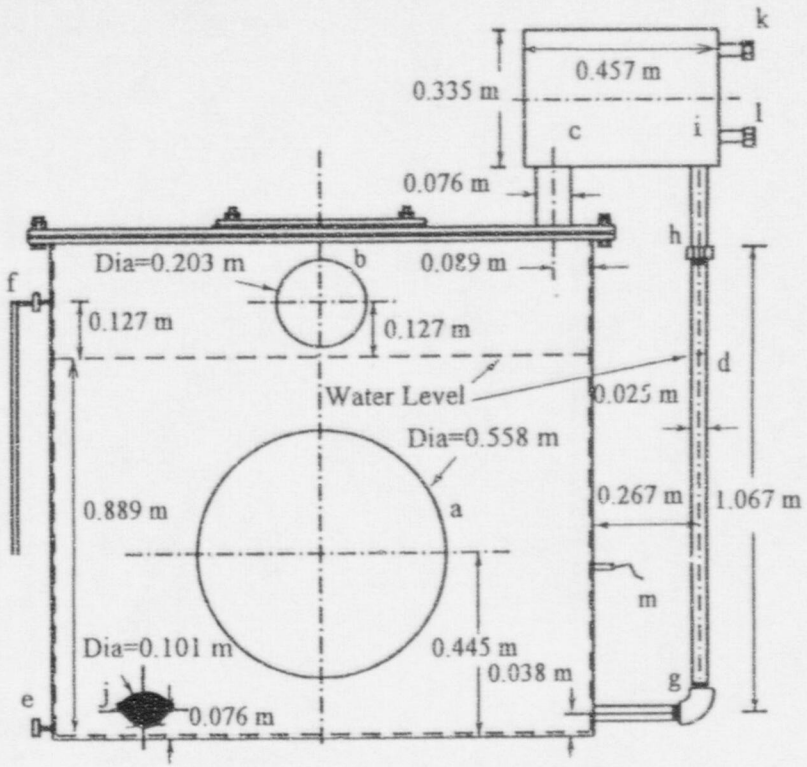

a Viewing Window
b Viewing Window
c Condenser
d Condensate Return
e Drain
f Water Inlet and Pressure Relief Valve
g Elbow
h Pipe Connection
i Condenser Access Door
j Immersion Heater
k Cold Water Inlet
l Hot Water Outlet
m 2.54 mm dia Tube for thermocouples

Figure 2.1 Dimensions of the Water Tank with a Condenser Unit Employed in the Experiment.

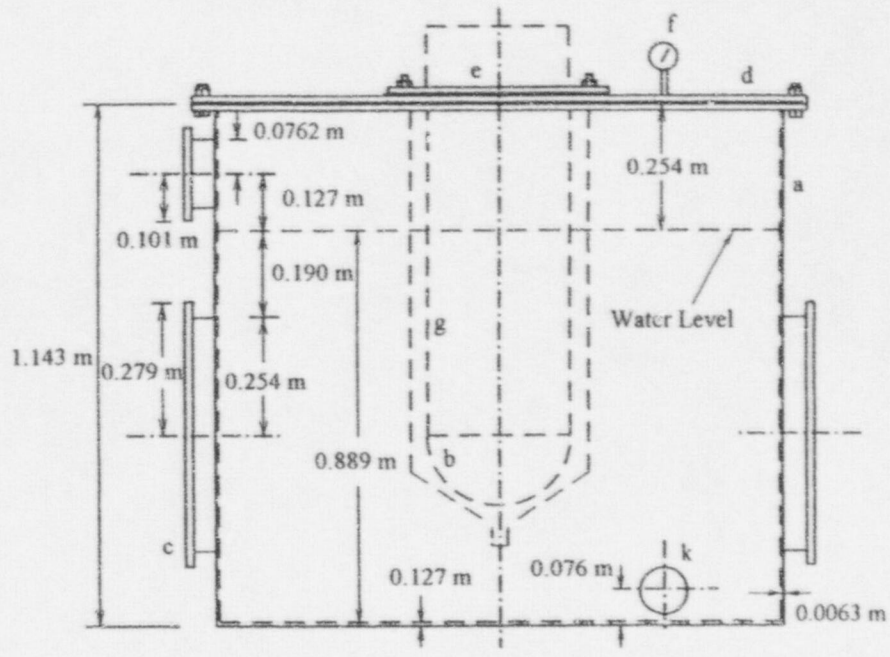

a Cylindrical Tank
b Hemisphere
c Viewing Window
d Tank Cover
e Tank Access Hole Cover
f Pressure Gage
g Large Cylindrical Pipe
k Immersion Heater

Figure 2.2 Schematic of the Simulated Reactor Vessel Surrounded by a Scaled Insulation Structure in the Water Tank

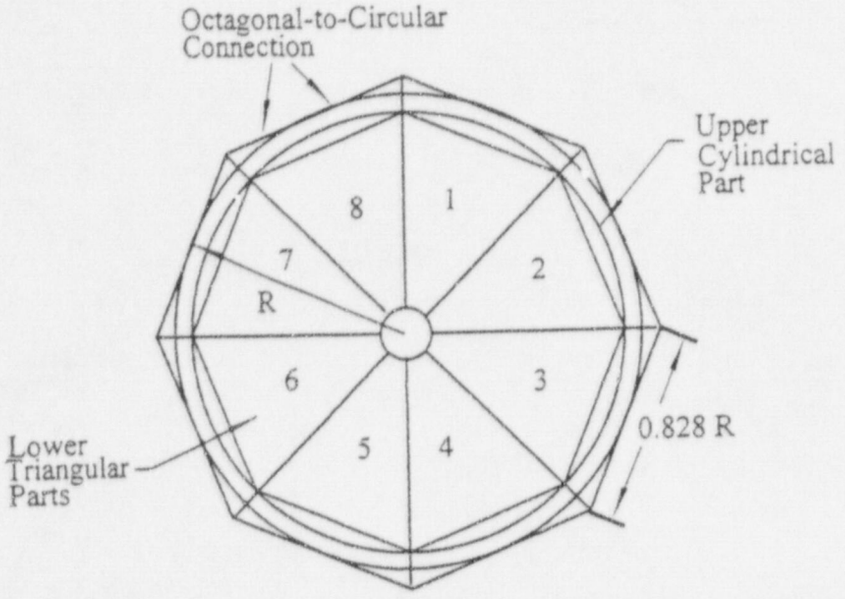

Figure 2.3 Top View of the Scaled Thermal Insulation Structure Showing the Connection Between the Upper Cylindrical and the Lower Octagonal Parts

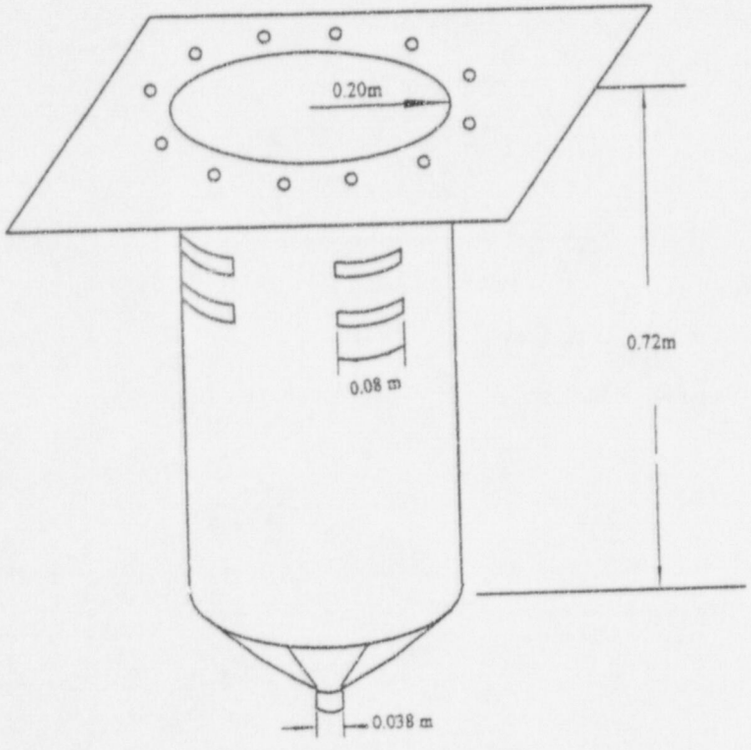

Figure 2.4 Side View of the Scaled Thermal Insulation Structure Showing the Two Sets of Horizontal Slots for Venting of Water and Steam.

was turned on for a short while (usually one to two minutes) to bring it back up. Before each experiment, the water was given time to become completely quiescent.

2.3 Measurement Techniques

Twenty K-type thermocouples were embedded at various locations inside the hemispherical lower part of the test vessel for temperature measurements. The thermocouple signals were recorded by using an IBM compatible personal computer along with a data acquisition system. Two Strawberry Tree ACPC-16 boards were installed inside the PC. Each board had 16 analog inputs and 16 digital input/output channels. The system was capable of monitoring up to 32 thermocouple signals. The ACPC-16 board was capable of resolutions in the range between 12 and 16 bits, which was equivalent to 0.024% and 0.0015% of full scale, respectively. Each of the boards had six voltages ranges that could be set according to the sensor used. The boards also had a high noise rejection integration converter, which helped reject 50/60 Hz AC power line interference when used in the "low noise mode". The ACPC-16 units were also capable of accurate cold junction compensation and linearization for thermocouple devices. The two ACPC-16 boards were connected to a total of four Strawberry Tree T12 boards, which in turn were connected to the thermocouples. Each of the T12 boards had 8 analog inputs and 8 digital input/output channels.

For steady-state boiling experiments, the speed of the data collection was not critical. Therefore, the slower program Quicklog developed by Strawberry Tree was employed to monitor the changes in the vessel temperatures. Quicklog was also used to read and store the local temperatures of the vessel at various locations inside the vessel wall. The recorded temperatures were then analyzed using an in-house inverse heat conduction code [2] to determine the local boiling heat fluxes and the local wall superheats. For heat flux levels above 0.1 MW/m^2, which is the range anticipated under severe accident conditions, the relative error in the heat flux measurement was estimated to be ±7%.

The photographic system consisted of a Minolta X-370 high speed camera and a Kodak Ektapro high speed video system. The camera could be set to a speed as high as 1000 frames/sec with an appropriate lighting level. The high speed video system consisted of a motion analyzer, an imager, a cassette conditioner and a TV set. The motion analyzer was used to set the speed of videotaping to a value as high as 1000 frames/sec. Once a session was recorded, the motion analyzer was used to play the recorded boiling phenomenon on the TV screen. In addition, it was possible to play the event one frame at a time, which was very helpful in studying the characteristics of the vapor dynamics on the vessel outer surface.

When the critical heat flux was reached during steady state heating experiments, any further increase in the power input could result in the onset of film boiling. This was characterized by a sudden large increase in the temperature of the heating surface. In order to protect the vessel against any possible meltdown, a control mechanism was installed to discontinue the power supply to the heaters when a significant jump in the vessel temperature was detected in the high heat flux regime. The power control system consisted of a data acquisition system, a constant DC power source, a solid state relay, and thermocouples to measure the vessel wall temperature, as shown in Figure 2.5. The

solid state relay had a low voltage side connected to the constant DC power source, and a high voltage side connected to the variac supplying the heaters. The solid state relay was needed because the high voltage of the variac could not be connected directly to the digital I/O channel of the data acquisition board. When a wall temperature greater than the set point value of 180°C was detected, the digital I/O channel became open. As a result, the low voltage side of the solid state relay was not powered anymore and the power supply to the heaters was discontinued, which prevented any further substantial increase in the vessel wall temperature. This also allowed the critical heat flux to be directly determined.

2.4 References

1. Cheung, F. B., Haddad, C. K. and Liu, Y. C., "Critical Heat Flux (CHF) Phenomenon on a Downward Facing Curved Surface," NUREG/CR-6507, U. S. Nuclear Regulatory Commission, Washington, D. C., 1997.

2. Y. C. Liu, "Inverse Heat Conduction in a Segmented Hemispherical Vessel with Downward Facing Boiling Boundary Conditions," *M. S. Thesis*, Pennsylvania State University, University Park, PA, 1995.

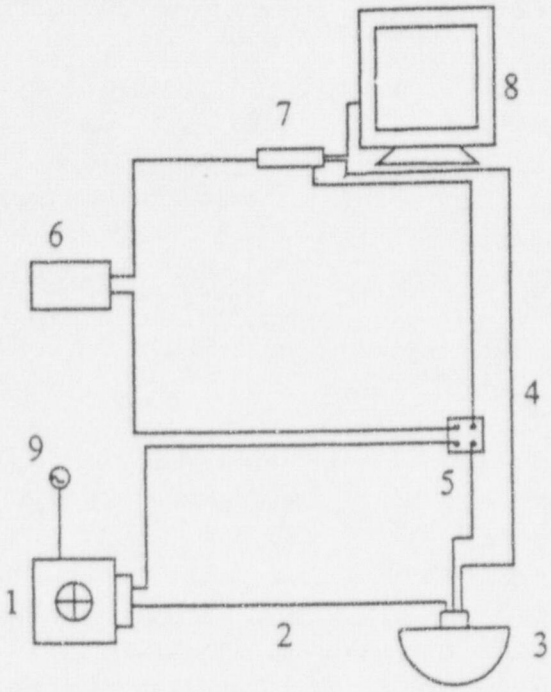

1 Power variac
2 Electric wire
3 Test Section
4 Thermocouple wire
5 Solid state relay
6 DC power source

Figure 2.5 Schematic of the Power Control System Used to Detect the Occurrence of CHF on the Vessel Wall

3. ANALYSIS OF THE UPWARD CO-CURRENT FLOW INDUCED BY THE NATURAL CONVECTION BOILING PROCESS

From the literature survey in Appendix A, it is known that the presence of gas-liquid flow inside channels is an extremely complex phenomenon since the flow conditions in a channel vary along its length, over it cross section, and with time. This is especially true as the two-phase motion is induced by and strongly coupled to the natural convection boiling process in the present case. Thus the problem becomes a three-dimensional periodic one corresponding to the boiling cycle, involving two phases, the full analysis of which is beyond the scope of this study. Therefore it is desired to seek a simplified picture of the problem which can be analyzed and yet, retains important features of the flow. The model presented here is that of one-dimensional flow. The objective is to predict the entrained rate of flow induced by the natural convection boiling process on the vessel outer surface.

In this model, it is assumed that the flow conditions in each phase vary only with distance along the channel, as depicted in Figure 3.1. This is a sweeping simplification of the true flow conditions and the reader must be fully aware that this can give rise to some uncertainties. Despite this, when used with care the model may provide useful flow information and is relatively easy to use.

3.1 The Continuity Equation

The void fraction is commonly taken as the fraction of volume occupied by the gas phase in the flow channel. The one-dimensional flow assumption means that the void fraction α is the fraction of flow area occupied by the gas phase:

$$A = A_v + A_l \;\; ; \;\; \alpha = \frac{A_v}{A} \;\; ; \;\; 1-\alpha = \frac{A_l}{A} \qquad (3.1)$$

where A_v and A_l are the cross-sectional area occupied by the gas and liquid phase respectively and A is the total cross-sectional area of the channel. The vapor flow rate $\dot{m}_v$ is given by

$$\dot{m}_v = \rho_v u_v A_v \;\; ; \;\; x = \frac{\dot{m}_v}{\dot{m}} \;\; ; \qquad (3.2)$$
$$\dot{m} = \dot{m}_v + \dot{m}_l = constant$$

where x is the vapor-phase mass flow fraction, ρ_v the vapor density, u_v the vapor velocity, and $\dot{m}$ the total mass flow rate.
Similarly, for the liquid phase, the liquid velocity and the liquid mass flow rate are given by

$$\dot{m}_l = \rho_l u_l A_l \qquad ; \qquad 1-x = \frac{\dot{m}_l}{\dot{m}} \qquad (3.3)$$

The local flow length dz, the hydraulic diameter D_h, and the mass velocity G of the two-phase mixture are given respectively by:

$$dz = \sin\Omega ds \;\; ; \;\; D_h = \frac{4A}{P} \;\; ; \;\; G = \frac{\dot{m}}{A} \qquad (3.4)$$

where Ω is the local angle of inclination of the channel and ds is the local length of inclination of the channel. Note that the channel under consideration (see Figure 3.2) has a non-uniform cross-sectional area A and thus, A, P, and G would vary along the flow direction in the channel.

3.2 The Momentum Equation for One-dimensional Two-phase Flow

A force balance over the element of volume depicted in Figure 3.1 for two-phase flow yields

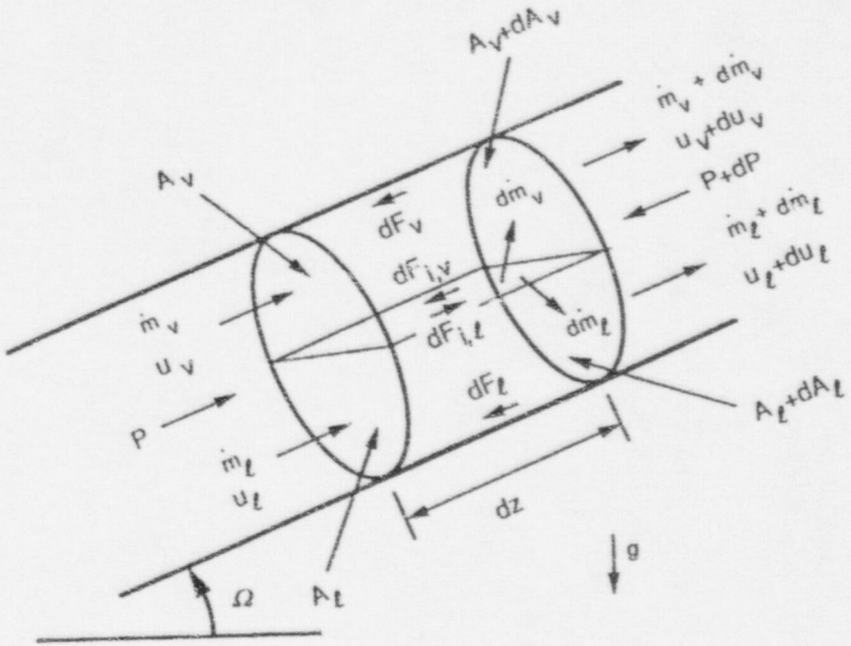

Figure 3.1 Schematic of the Important Flow Quantities in the Flow Channel Considered in the One-Dimensional Analysis.

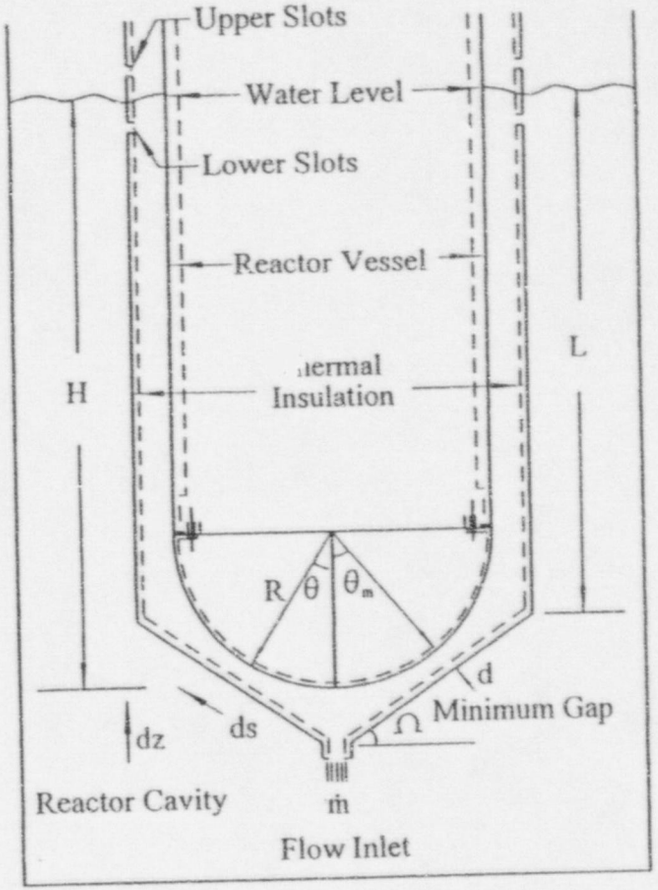

Figure 3.2 Schematic of the Annuiar Channel Formed Between the Scaled Reactor Vessel and the Thermal Insulation Structure.

$$-\left(\frac{dp}{ds}\right)=\frac{4\tau_w}{D_h}+[(1-\alpha)\rho_l+\alpha\rho_v]g\sin\Omega$$
$$+G\frac{d}{ds}[xu_v+(1-x)u_l] \qquad (3.5)$$
$$+\left(\frac{dp}{ds}\right)_m+\frac{P}{A}\left(\frac{dA}{dz}\right)$$

where the last term on the right-hand side of the above equation represents the change of total pressure due to the change of cross-sectional area. It is expected that this term is of secondary importance. Wallis [1] simply neglected this term in deriving the momentum equation for one-dimensional two-phase flow. This term will be assumed negligible in our numerical analysis.

By expressing the above equation in integral form, we have

$$\rho_l gL=\int\left[\frac{4\tau_w}{D_h}+[(1-\alpha)\rho_l+\alpha\rho_v]g\sin\Omega\right.$$
$$+G\frac{d}{ds}[xu_v+(1-x)u_l] \qquad (3.6)$$
$$\left.+\left(\frac{dp}{ds}\right)_m\right]ds$$

With further simplifications, we obtain

$$\rho_l gL=-\int\left[\frac{4\phi_{lo}}{D_h}\left(\frac{dp}{ds}\right)_{lo}\right]ds \qquad (3.7)$$
$$+\int[(1-\alpha)\rho_l+\alpha\rho_v]gdz$$
$$+\int Gd[xu_v+(1-x)u_l]+\int(dp)_m$$

In deriving the above expression, we have employed the assumption of local equilibrium such that the pressure of the liquid phase is equal to that of the gas phase. The term on the left-hand side of equation (3.7) represents the total liquid head above the bottom flow inlet. The first term on the right-hand side represents the pressure drop due to two-phase frictional force on the channel wall. The second term represents the gravitational pressure drop. The third term represents the pressure drop due to acceleration of flow. The cause of acceleration of flow could be attributed to phase change and change of cross-sectional flow area. The last term represents the pressure drop due to the sudden change of geometrical characteristics including sudden contraction at the entrance and sudden expansion at the exits of the channel under consideration.

3.3 The Energy Equation for One-dimensional Two-phase Flow

An energy balance over the element of volume depicted in Figure 3.1 for two-phase flow yields:

$$\frac{1}{\dot{m}}\left(\frac{d\dot{Q}}{ds}-\frac{d\dot{W}}{ds}\right)=\frac{d}{ds}[xh_v+(1-x)h_l] \qquad (3.8)$$
$$+\frac{d}{ds}\left[x\frac{u_v^{\,2}}{2}+(1-x)\frac{u_l^{\,2}}{2}\right]+g\sin\Omega$$

where the above equation was derived by ignoring axial conduction, heat transfer due to the oscillation of the medium, and frictional losses (viscous dissipation) in the energy equation.

Comparing to the enthalpy change upon evaporation, the changes of kinetic energy and potential energy are negligible. There is no work done by either the fluids or surrounding. Hence, the work term is dropped out. Under saturated boiling conditions, the above equation can be simplified to:

$$x = \frac{\dot{Q}}{\dot{m}h_{lv}} = \frac{\pi D^2}{2\dot{m}h_{lv}} \int_0^{\theta} \dot{Q}'' \sin\theta d\theta \qquad (3.9)$$

3. 4 Two-Phase Frictional Pr[illegible] Drops

The wall shear stress due to the two-phase pressure drops in the flow direction is related to the two-phase multiplier as expressed below:

$$\tau_w = -\left(\frac{dp}{ds}\right)_{fr} = -\phi_{lo}^2 \left(\frac{dp}{ds}\right)_{lo} \qquad (3.10)$$

$$\left(\frac{dp}{ds}\right)_{lo} = -\frac{f_{lo} G^2}{2\rho_l D_h} \qquad (3.11)$$

The friction factor for channel flow having a smooth wall in the turbulent flow regime can be correlated by the following power-law equation of Sadatomi & Sato [2] similar to Blausius:

$$f_{lo} = C_t \, \mathrm{Re}_{Dh}^{-0.25} \qquad (3.12)$$

where C_t is termed as the geometry factor for turbulent flow and *lo* the frictional pressure gradient that would result if liquid only flows through the channel at the same total mass flow rate.

The value of C_t is given by Sadatomi & Sato [2] as follows:

$$\frac{C_t}{C_{lo}} = \sqrt{\left(0.0154 \frac{C_l}{C_{lo}} - 0.012\right) + 0.85} \qquad (3.13)$$

The two-phase multiplier ϕ_l can be determined from the correlation derived by Chisholm and Laird [3] for upward co-current two-phase flow, whereas the Martinelli parameter, X_{tt} is employed for vapor and liquid both flowing turbulently alone:

$$\phi_l = \left(1 + \frac{21}{X_{tt}} + \frac{1}{X_{tt}^2}\right)^{1/2} \qquad (3.14)$$

$$X_{tt} = \left(\frac{\rho_v}{\rho_l}\right)^{0.5} \left(\frac{\mu_l}{\mu_v}\right)^{0.125} \left(\frac{1-x}{x}\right)^{0.875} \qquad (3.15)$$

Because the quantity ϕ_{lo} is used in the numerical analysis, it is necessary to know the relationship between ϕ_{lo} and ϕ_l. This relationship is derived as follows:

$$\phi_l = \left[\frac{(dP/dz)_{fr}}{(dP/dz)_l}\right] \quad ; \qquad (3.16)$$

$$-\left(\frac{dP}{dz}\right)_l = \frac{fG^2(1-x)^2}{2\rho_l D_h}$$

$$\phi_{lo} = \left[\frac{(dP/dz)_{fr}}{(dP/dz)_{lo}}\right] \quad ; \qquad (3.17)$$

$$-\left(\frac{dP}{dz}\right)_{lo} = \frac{f_{lo} G^2}{2\rho_l D_h}$$

and $$f = C_t \left(\frac{GD_h}{\mu}\right)^{-0.25} \qquad (3.18)$$

The final result of derivation is:

$$\phi_{lo}^2 = \phi_l^2 (1-x)^{1.75} \qquad (3.19)$$

Zivi's (1964)correlation is adopted here for the void fraction α in the present numerical calculations:

$$\alpha = \left[1 + \left(\frac{1-x}{x}\right)\left(\frac{\rho_v}{\rho_l}\right)^{0.67}\right]^{-1} \qquad (3.20)$$

Note that the choice of the above correlation for the void fraction is not at all arbitrary.

The void fraction for downward facing boiling in the channel heated on the downward facing side under consideration is expected to change from its minimum value of nearly zero at the bottom center to its maximum value of ~0.9 at the equator of the test vessel. Therefore, the criterion of choosing a correlation must be met with this condition.

3.5 Other Pressure Drops

There are three types of minor pressure drops due to sudden contraction at the entrance, sudden expansion at the exit, and gradual conical expansion losses, respectively. The following correlations is adopted from White (1994).

$$(\Delta p)_m = K\left(\frac{1}{2}\rho_l u_l^{\,2}\right) \qquad \textbf{(3.21)}$$

where the coefficient K is given by

$$K_{SE} \approx \left(1-\frac{d^2}{D^2}\right) \qquad \textbf{(3.22)}$$

and

$$K_{SC} \approx 0.42\left(1-\frac{d^2}{D^2}\right) \qquad \textbf{(3.23)}$$

In the above expression, K_{SC} represents the coefficient for sudden contraction and K_{SE} the coefficient for sudden expansion. In the cases of sudden expansion and contraction, d, the diameter of the channel before the flow experience a sudden geometrical change due to sudden expansion, (or the diameter after the flow experience a sudden geometrical change due to sudden contraction) is much smaller than D, the diameter of the reservoir in this case. Therefore, $(d/D)^2$ can be neglected as it is much less than unity.

For a cone angle greater than 60°, the loss is so excessive that it would actually be better to use a sudden expansion. Therefore in our case, the correlation for sudden expansion is used here for obtaining pressure loss due to a gradual conical expansion.

3.6 Numerical Solution Scheme

If every quantity given in the momentum equation is known, the total mass flow rate including the liquid entrainment can be obtained by balancing the momentum equation, providing the total pressure drop is given. However, the two-phase pressure drop, the accelerational pressure drop, and the gravitational pressure drop all depend on the induced mass flow rate. Therefore, an iterative scheme based on the Secant method is used to solve for the induced mass flow rate from the momentum equation.

To facilitate the numerical computation, a systematic approach is used to choose the initial trial value for the mass flow rate. This is needed in order to prevent the divergent results of calculation. The approach adopted here involves the use of the Bisection method. As shown in Figure 3.3, two subroutines and one function have been set up as the frame structure of the program. These are the subroutine Bisection, the subroutine Secant, and the function Mass-Momentum. The subroutine Bisection is used to check if the range of mass flow rate is valid that it contains at least a root to the function and if it is not, the subroutine will return a valid range to the program. The subroutine Secant is used to find the roots of the function. Function Mass-Momentum is used to implement the above root-finding and range-checking tasks. The computer algorithm so developed is listed in Appendix B.

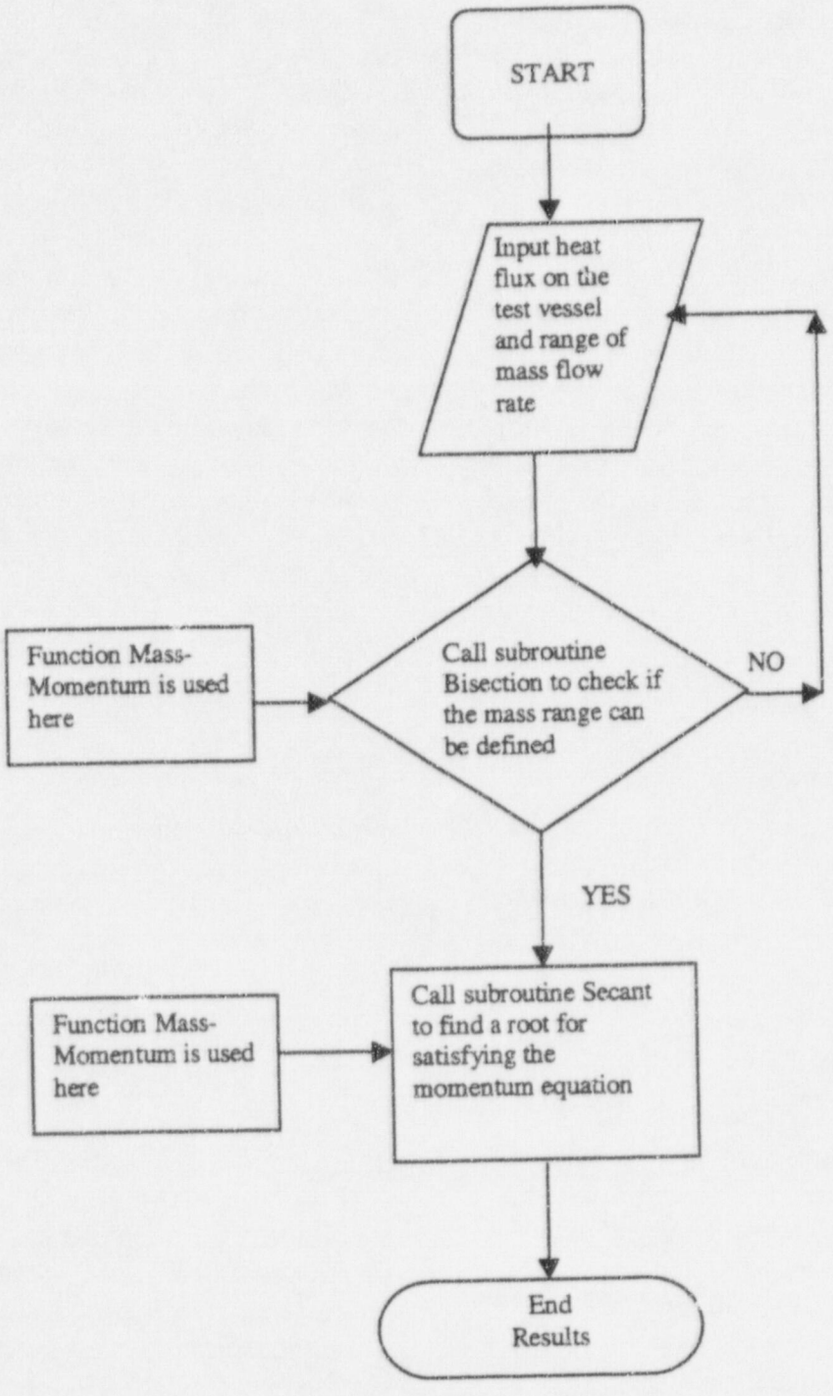

Figure 3.3 Flow Chart for Calculating the Mass Flow Rate from the Momentum Equation

3.7 Reference

1. Wallis, G. B., "One-Dimensional Two-Phase Flow", Wiley, New York, 1965.

2. Sadatomi, M. and Y. Sato, "Two-Phase Flow in Vertical Noncircular Channels," *Int. J. Multiphase Flow*, Vol. 8, No. 6, FP. 641-655, 1992.

3. Chisholmm D. and A. D. Laird, "Two-Phase Flow in Rough Tubes," Trans. ASME, Vol. 80, PP. 276-286,1958.

4. Zivi, S. M., "Estimation of Steady-State Steam Void-Fraction by Means of the Principle of Minimum Entropy Production," *J. Heat Transfer*, Vol. 86, PP. 247-252, 1964.

5. White, F. M., "Fluid Mechanics," McGraw-Hill, Inc., 1994.

3.8 Nomenclature

A	Cross sectional area of the flow channel
C	Geometry factor associated with frictional loss
d	Channel diameter
D	Outside diameter of the vessel or channel diameter employed in correlation for minor pressure drop
D_h	Hydrodynamic diameter of the channel
ds	Local length of the inclined channel
dz	Local vertical length of the channel
f	Friction factor
g	Acceleration due to gravity (m/s^2)
G	Mass flux
h	Enthalpy of the fluid
h_{fg}	Latent heat of vaporization
K	Coefficient associated with pressure drop
L	Water column height on the outside of the reactor lower head
$\dot{m}$	Total mass flow rate
P	Periphery of the flow channel
$\dot{Q}$	Total heat generated by downward-facing boiling
Re	Reynolds Number
$\dot{W}$	Work done by the fluid flowing in the channel
x	Mass fraction of vapor
Δp	Pressure drop

Greek Symbols

α	Local void fraction
Ω	Local angle of inclination of channel
ϕ	Two-phase multiplier
μ	Viscosity
ρ	Density (kg/m^3)
τ	Shear stress (N/m^2)
θ	Angular position measured from the bottom center of the vessel
θ_m	Minimum gap location

Subscript

CHF	Quantities at the CHF point
fr	Quantities associated with frictional loss
l	Fractional quantities for liquid flowing alone through the channel
lo	Quantities for liquid only flowing through the channel at the same total mass flow rate
m	Minimum or minor
sat	Saturation quantities
sc	Sudden contraction
se	Sudden expansion
t	Turbulent Flow
tt	Liquid and vapor both flowing turbulently alone

v	Fractional quantities for vapor flowing alone through the channel
w	Wall quantities

4. RESULTS AND DISCUSSION

Steady-state natural convection boiling experiments were conducted under both saturated and subcooled conditions with the ambient water temperature of the tank varying from 90° to 100°C and with the system maintained at one atmospheric pressure. The vapor dynamics on the hemispherical lower part of the test vessel and the resulting two-phase flow phenomenon in the hemispherical annular channel were observed over the entire range of nucleate boiling with special emphasis on the high-heat-flux regime. Heat transfer data were collected at five separate locations along the downward-facing hemispherical surface. These data included the local boiling heat fluxes and the corresponding local wall superheats which can be used to construct the local nucleate boiling curves.

4.1 Vapor Dynamics and Two-Phase Flow Phenomenon

Photographic studies were performed to seek a clear physical understanding of the vapor dynamics and two-phase flow through the annular gap between the test vessel and the scaled insulation structure under steady-state boiling conditions. When the water was subcooled at 90°C and the heat flux level was relatively low (i.e., below 0.07 MW/m^2), the outer surface of the hemispherical test vessel was covered with a large number of tiny vapor bubbles. The bubbles were isolated from each other and there was no coalescence. Four separate stages of the bubble formation process were observed. The process started with the heating of the subcooled liquid in contact with the heating surface during the waiting period. When the required local level of superheat was attained, the nucleation site became active and a very tiny bubble could be observed on the local heating surface. The vapor mass then grew larger and larger as more liquid was evaporating at the surface. Finally, the vapor mass detached from the surface when surface tension force could no longer hold it in place. The resulting two-phase motion in the annular channel, being driven by buoyancy, was evidently in the bubbly flow regime.

As the local heat flux was increased, the frequency of the bubble generation increased. The size of the vapor masses became much larger and the bubbles were no longer spherical in shape. Rather, they became elongated especially for those that were growing near the bottom center region. Furthermore, the bubbles appeared to interfere with the adjacent ones and tended to coalesce with each other. When the heat flux was increased beyond 0.4 MW/m^2, the frequency of bubble generation became very high and the adjacent bubbles tended to coalesce to form one or several large elongated vapor masses. These large elongated vapor masses then ejected upward from underneath the hemispherical test vessel. They then quickly condensed to smaller vapor masses as they traveled upward through the annular gap. The resulting two-phase motion in the annular gap appeared to be in the slug flow regime.

When the heat flux was further increased to 1.0MW/m^2, the bubble formation frequency became so high that the external bottom surface of the test vessel was covered by a single elongated vapor mass. This single large vapor mass expanded upward in a cyclic manner to form a ring as it covered the downstream locations. It then broke into several slugs in random directions as it detached from the downward-facing heating surface. The slugs quickly condensed as they flow upward in the annular channel.

The resulting two-phase motion appeared to be in the churn turbulent regime.

When the water was saturated at 100°C, the bubble dynamics and the flow activities were much more vigorous than those under subcooled conditions. At the same heat flux level, the bubble sizes were almost an order-of-magnitude larger and they were more readily to coalesce with each other. Moreover, they do not condense to smaller bubbles as they flow upward through the annular channel. This resulted in a much larger liquid entrainment and a considerably higher mass flow rate. Video records showed that large elongated vapor masses or slugs, being squeezed against the wall by the local buoyancy force, grew periodically on the vessel outer surface. They were then ejected violently upward in all directions, resulting in an upward co-current two-phase flow through the annular channel. The two-phase motion appeared to be in the churn turbulent regime. Close observation of the flow clearly revealed that it was three-dimensional with swirl formation when boiling was taking place at high-heat-flux levels. Strong upstream influences were observed as a result of the activities of large elongated bubbles in the bottom center region of the vessel.

It is worthy of noting that there was a minimum gap between the lower octagonal part of the scaled insulation structure and the hemispherical test vessel, as can be seen in Figures 1.1 and 2.2. The two-phase flow was accelerated as it passed through the minimum gap. Close observation of the two-phase flow phenomenon in the minimum gap region was made at high heat flux levels. Large vapor slugs, occupying nearly the entire cross-sectional flow area, were observed to flow through the minimum gap in a highly unsteady and chaotic manner. This unsteady, chaotic feature was probably caused by the high-frequency cyclic vapor ejection process associated with the downward facing boiling on the external bottom surface of the test vessel and the three-dimensional swirls generated by the strong recirculation motions in the annular channel. This unsteady, chaotic feature of the two-phase motions gave rise to a significant flow-induced vibration of the lower octagonal part of the insulation structure.

4.2 Numerical Prediction of the Upward Co-current Flow

The numerical scheme described in Section 3 is carried out by assuming uniformly distributed heat flux along the heating surface from the bottom center to the equator of the vessel. The induced mass flow rates for heat fluxes from 0.1 to 1.0 MW/m^2 have been determined in the numerical calculations to investigate the effect of the heat fluxes on the mass flow rate. The magnitudes of various contributions on the total pressure drops for various heat fluxes are also determined in the analysis.

The predicted mass flow rates are plotted against the heat fluxes in Figure 4.1 for three different minimum gap sizes of the channel. For a given minimum gap size, the induced mass flow rate increases as the input heat flux is increased until the heat flux becomes larger than 0.7 MW/m^2 . When the heat flux is increased beyond 0.7 MW/m^2, the total mass flow rate decreases moderately with increasing heat flux. Physically, the increase in the total mass flow rate with increasing heat flux is due to the liquid entrainment by the vapor flow. The more liquid mass is consumed due to boiling of liquid, the more the mass flow rate is "entrained" from the bottom inlet of the thermal insulation. However, the total mass flow rate does not

increase monotonically with the heat flux. This is mainly due to the increase in the two-phase pressure drop as the induced mass flow rate and the heat flux are increased. From equations (3.10) and (3.11), it can be seen that the two-phase pressure drop is proportional to ϕ_{lo}^2 , f_{lo} , and G^2 ; furthermore, ϕ_{lo}^2 is proportional to $x^{0.75}$ and f_{lo} is proportional to $G^{-0.25}$. The proportionality expressed in terms of x and G for the two-phase pressure drop is $x^{0.75}\ G^{1.75}$. Therefore, as the quality and the induced mass flow rate are increased, the two-phase pressure drop will increase. This in turn will reduce the amount of liquid entrained from the bottom inlet. The critical mass flow rate corresponds to the maximum two-phase pressure drop that can be overcome by the buoyancy force. Note that at a given heat flux, the induced mass flow rate increases as the minimum gap size is increased. This is expected since the two-phase pressure drop becomes smaller as the gap size becomes larger. The critical mass flow rate also increases with increasing gap size. The present numerical results are consistent with the critical mass flow rate reported by Xia et al. [1] for natural convection boiling in a vertical rectangular channel.

Figure 4.2 and 4.3 show the liquid flow rate and the vapor flow rate respectively, at various angular positions with the heat flux as a parameter. In these figures, it can be seen that the vapor flow rate and the liquid consumption rate go up quickly from the bottom center to the equator of the test vessel for heat fluxes above 0.6 MW/m^2. It is also worthy to note that the quality of the vapor in the channel is below 40 % for various input heat flux levels. The spatial variation of the void fraction with the angular position is shown in Figure 4.4 whereas the superficial vapor velocity is given in Figure 4.5. For heat fluxes equal to or larger than 0.5 MW/m^2, the void fraction increases very rapidly from zero at the bottom center to nearly unity at 40° downstream. The flow regimes in the channel is apparently in the slug flow regime around the bottom center for heat fluxes equal to or greater than 0.6 MW/m^2 according to the criterion of Mishima and Ishii [2]. Around the place where the minimum gap size is located (~45°), the superficial vapor velocity exhibits a local peak. The flow is apparently in the churn-turbulent flow regime according to Mishima and Ishii. This flow regime was confirmed by the present experimental observations.

From the results of numerical analysis, it is shown that the two-phase boundary layer flow in the channel is driven entirely by the buoyancy force under the influence of gravity with downward facing boiling conditions. The time scale ratio for buoyancy-controlled steam venting process [1] should be preserved in order to insure the prototypicality of the test data obtained in the experimental measurements. The results of numerical analysis further indicates that the two-phase frictional pressure drop increases profoundly with increasing mass flow rate and the input heat flux. This in turn may affect the boiling heat transfer and the critical heat flux.

4.3 Natural Convection Boiling Heat Transfer

The steady-state nucleate boiling data for the high-heat-flux regime measured at various locations of the test vessel are shown in Figures 4.6 to 4.10. In these figures, the local nucleate boiling heat fluxes are plotted against the local wall superheats with the water temperature as a parameter, which was varied in the experiments from 90°C for the case of subcooled boiling to 100°C for the case of saturated boiling. In contrast to

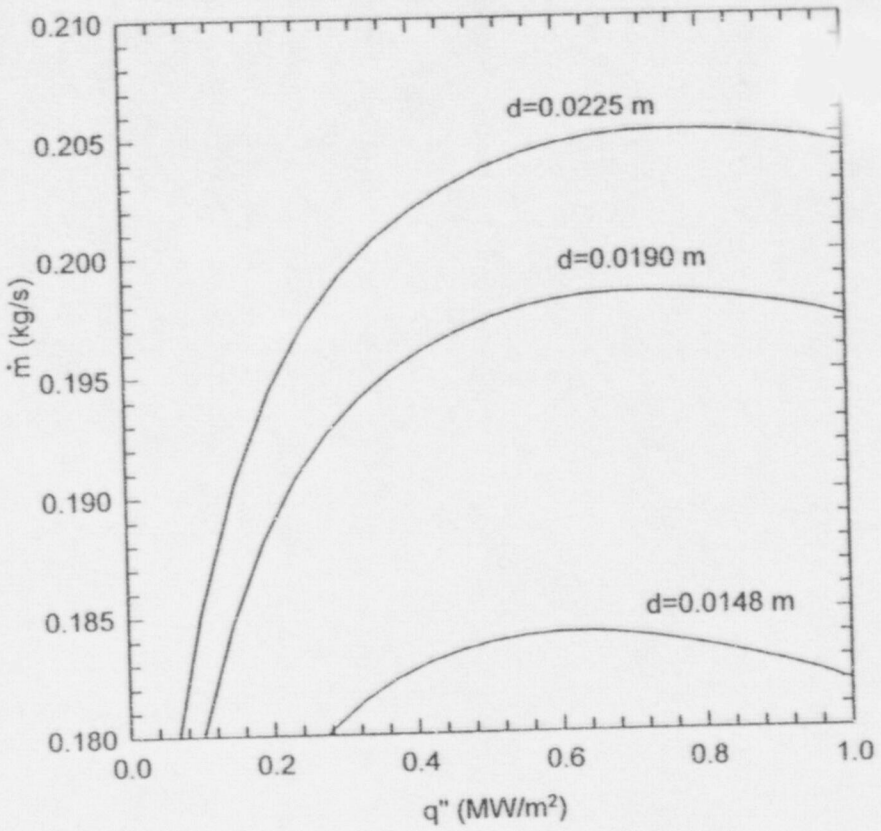

Figure 4.1 The Predicted Total Mass Flow Rate in the Annular Channel as a Function of the Heat Flux Level and the Channel Size.

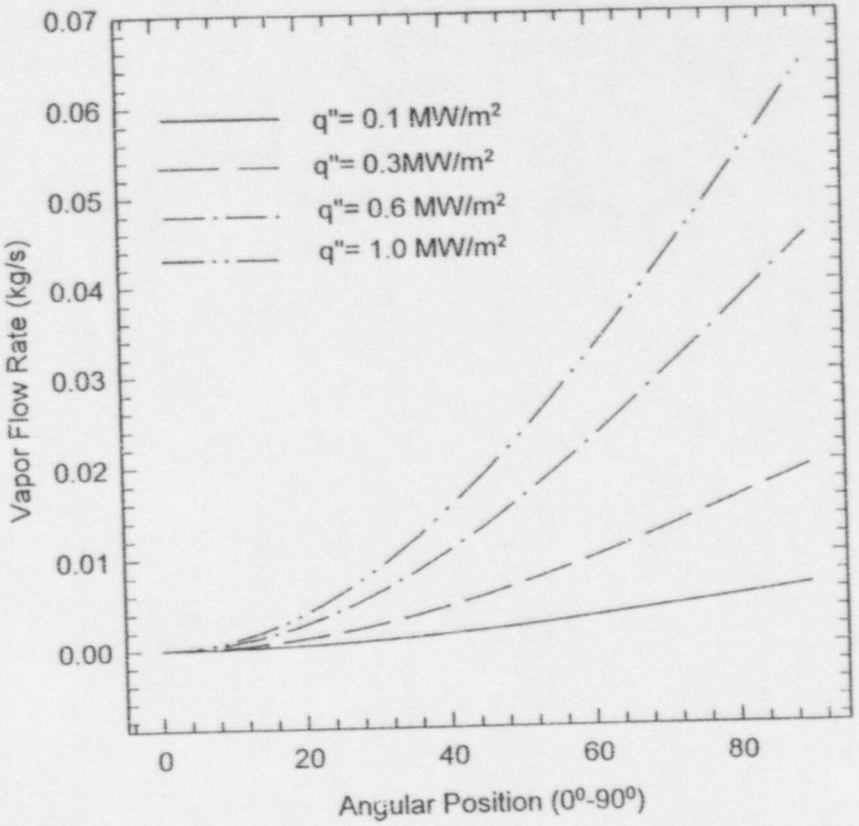

Figure 4.2 Spatial Variation of the Local Vapor Flow Rate Along the Vessel Outer Surface at Various Heat Flux Levels.

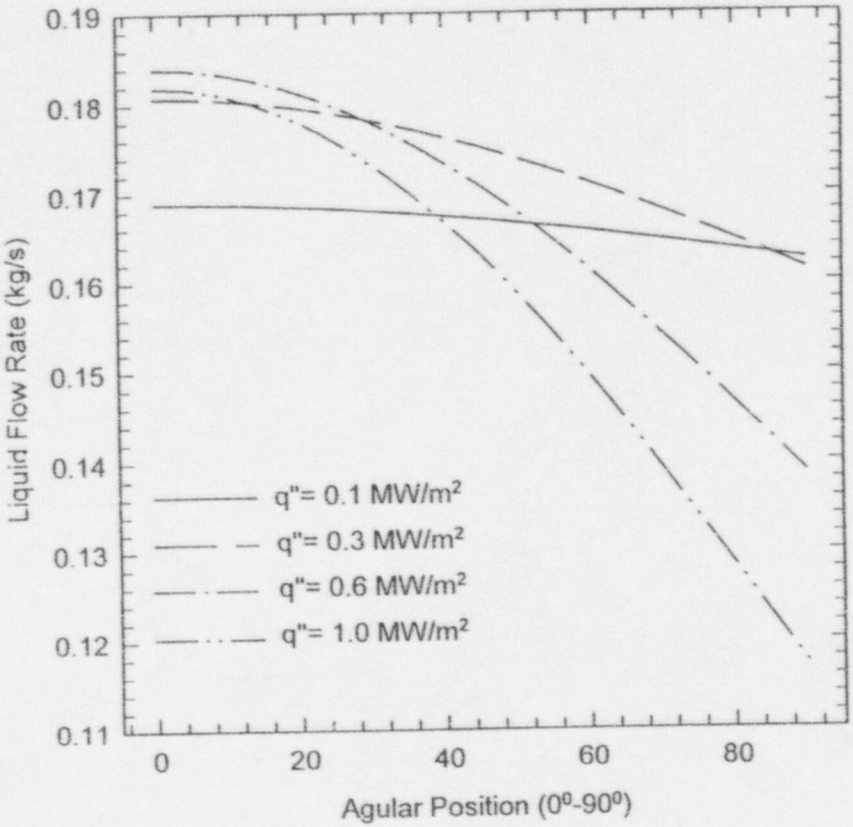

Figure 4.3 Spatial Variation of the Local Liquid Flow Rate Along the Vessel Outer Surface at Various Heat Flux Levels.

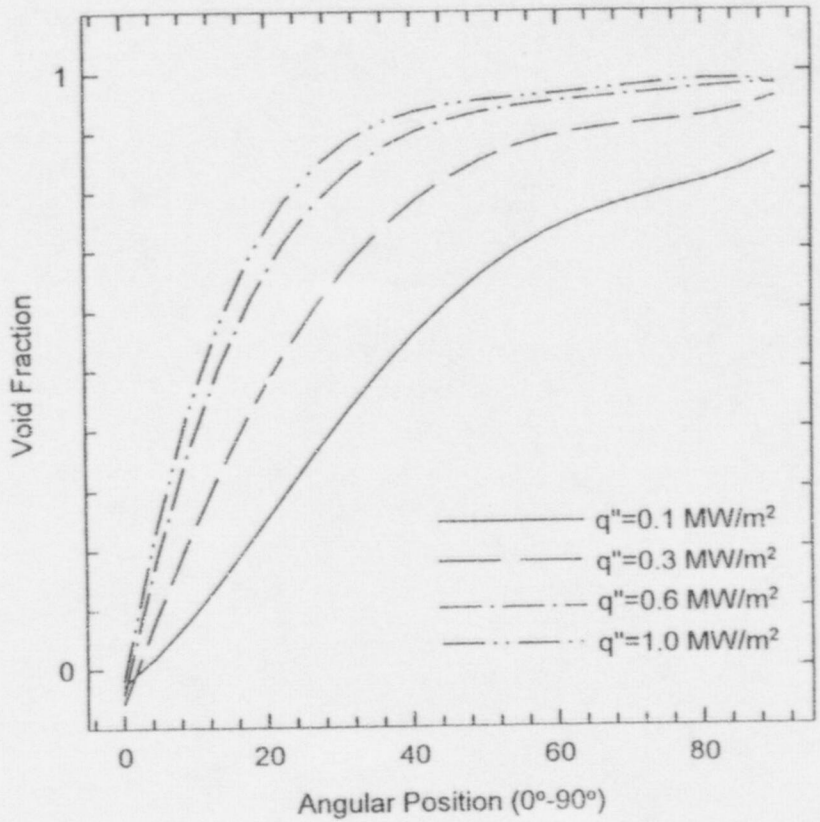

Figure 4.4 Spatial Variation of the Local Void Fraction in the Annular Channel at Various Heat Flux Levels.

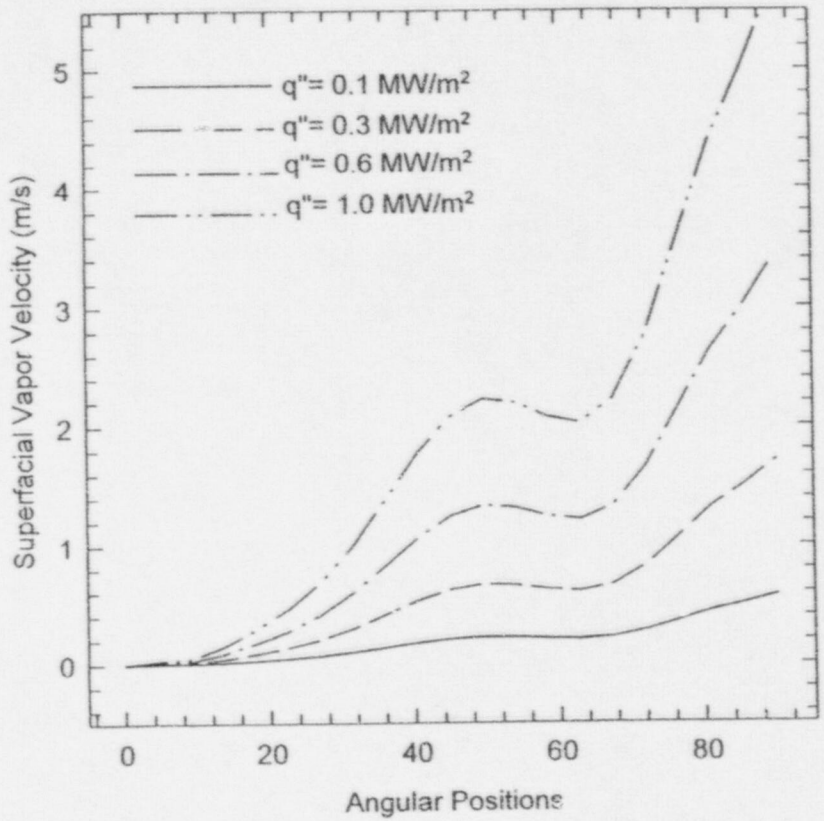

Figure 4.5 Spatial Variation of the Superficial Vapor Velocity Along the Vessel Outer Surface at Various Heat Flux Levels.

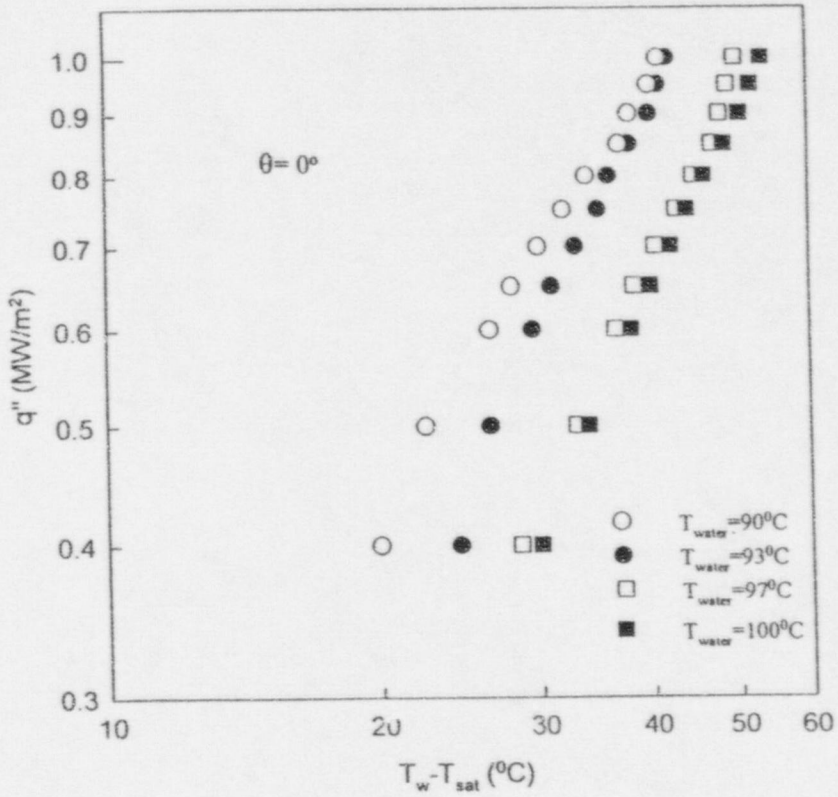

Figure 4.6 Natural Convection Boiling Data at the External Bottom Center of the Test Vessel (θ = 0°).

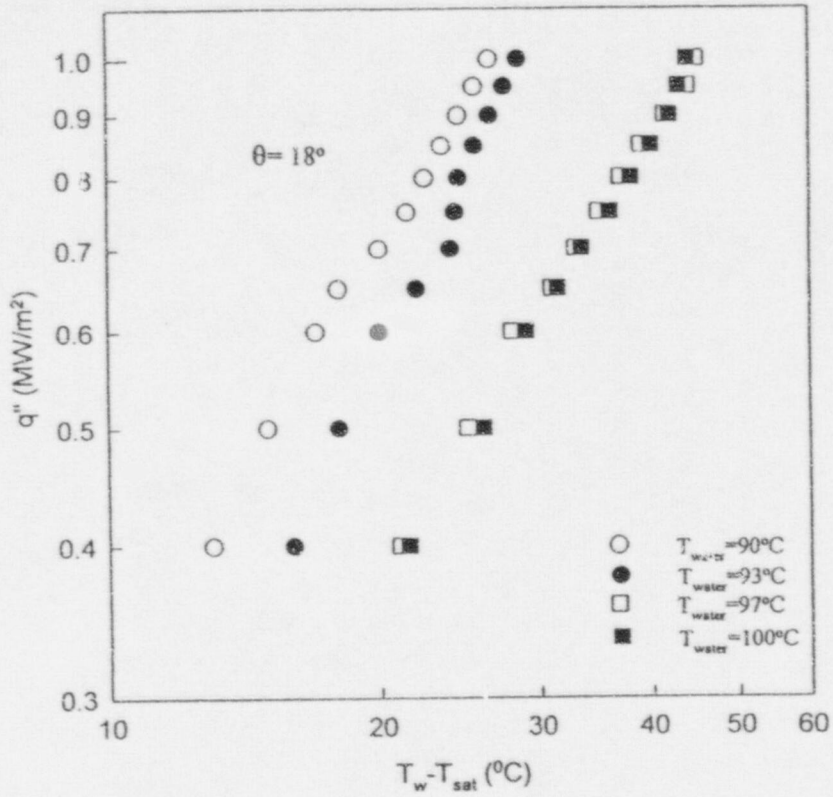

Figure 4.7 Natural Convection Boiling Data at an Off-Center Location of the Test Vessel (θ=18°).

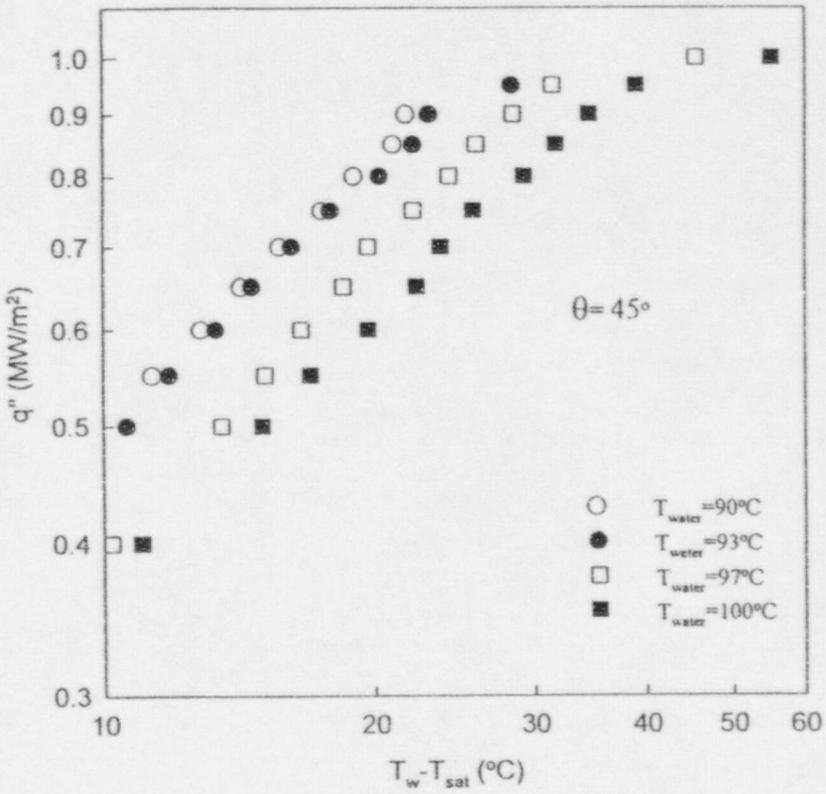

Figure 4.8 Natural Convection Boiling Data at an Off-Center Location of the Test Vessel (θ=45°).

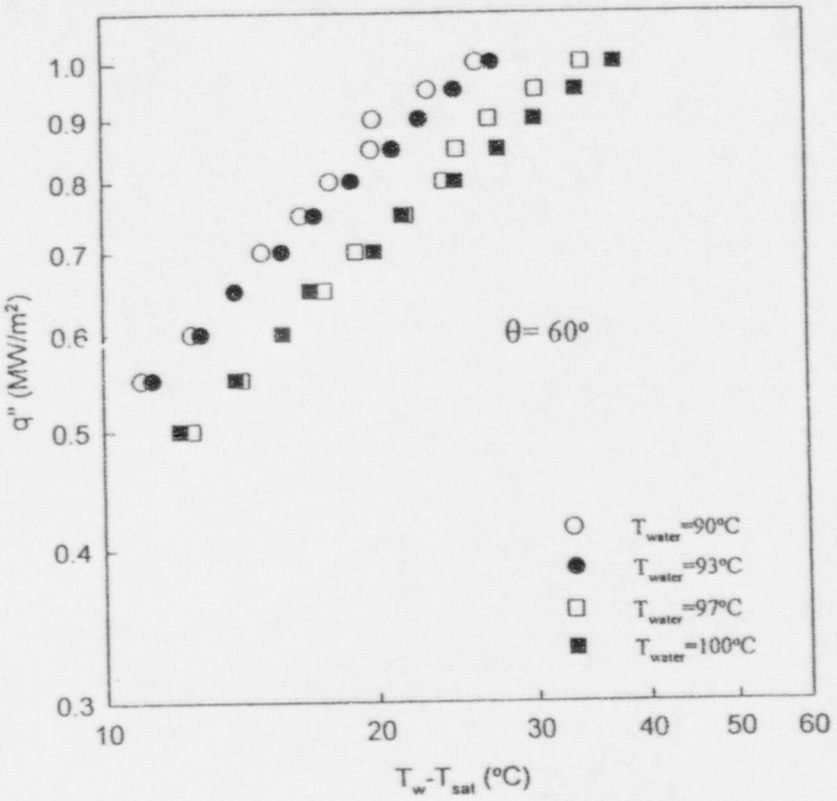

Figure 4.9 Natural Convection Boiling Data at an Off-Center Location of the Test Vessel (θ=60°).

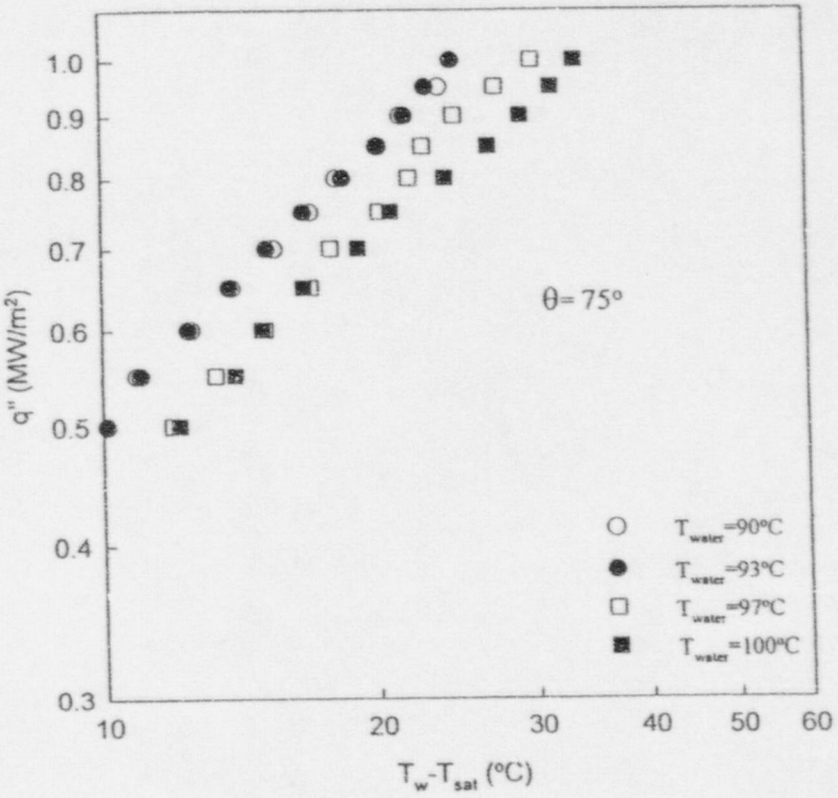

Figure 4.10 Natural Convection Boiling Data at an Off-Center Location of the Test Vessel (θ=75°).

the conventional case of pool boiling for which liquid subcooling has very little effect on nucleate boiling heat transfer, in the present case, a strong subcooling effect was observed at various locations of the vessel outer surface. The nucleate boiling curve in the entire high-heat-flux region shifted upward as the degree of subcooling was increased. Note that a strong subcooling effect was present in the entire high-heat-flux region. This behavior was different than that reported by Cheung, Haddad and Liu [3] for the case without an insulation where a significant subcooling effect was observed only at heat flux levels below 0.1 MW/m^2. This enhancement in the subcooled nucleate boiling heat transfer was evidently due to the effect of the upward co-current two-phase flow in the annular channel.

Because of the buoyancy-driven co-current two-phase flow that was induced by the boiling process, there was a significant variation of the nucleate boiling heat flux along the vessel outer surface. This was the case for both saturated and subcooled boiling, as shown in Figures 4.11 to 4.14. For a given water temperature, the nucleate boiling heat flux tended to increase in the downstream direction, evidently due to the natural convection flow effect. Although it was a pool boiling process, the phenomenon exhibited strong flow boiling characteristics. Note from Figures 4.8 and 4.11 that the nucleate boiling rate did not increase monotonically in the downstream location. Rather it underwent an adverse change in the minimum gap region. This adverse change was evidently due to the relatively large resistance to steam venting through the minimum gap.

The present results were compared to those corresponding data reported by Cheung, Haddad and Liu [3] for the case of "external" natural convection boiling on the outer surface of a hemispherical vessel without an insulation structure. It was found that under both saturated and subcooled boiling conditions, the nucleate boiling heat fluxes for the case with thermal insulation were consistently higher than the corresponding values for the case without thermal insulation. This difference in the nucleate boiling heat transfer was attributed to the buoyancy-driven two-phase flow effect. For the case without thermal insulation [3], an "external" natural convection two-phase boundary layer flow was induced by the boiling process. The mass flow rate increased in the downstream locations from its minimum value at the bottom center to its maximum value at the equator of the hemispherical vessel. Hence the flow effect was relatively weak in the bottom center region. On the other hand, an "internal" natural convection two-phase flow was induced by the boiling process in the present case with an insulation structure. Under steady-state boiling conditions, the mass flow rate was essentially constant throughout the entire flow channel. Hence the flow effect was relatively strong throughout the entire downward-facing hemispherical heating surface compared to the corresponding case without thermal insulation. This resulted in a higher heat transfer rate.

4.4 Spatial Variation of the Critical Heat Flux

For the case without thermal insulation, Cheung and Haddad [4] found that the local critical heat flux is a monotonically increasing function of the angular position on the vessel outer surface. It had a minimum value at the external bottom center of the vessel and a maximum value at the equator (i.e., upper edge) of the vessel. A radically different spatial variation of the

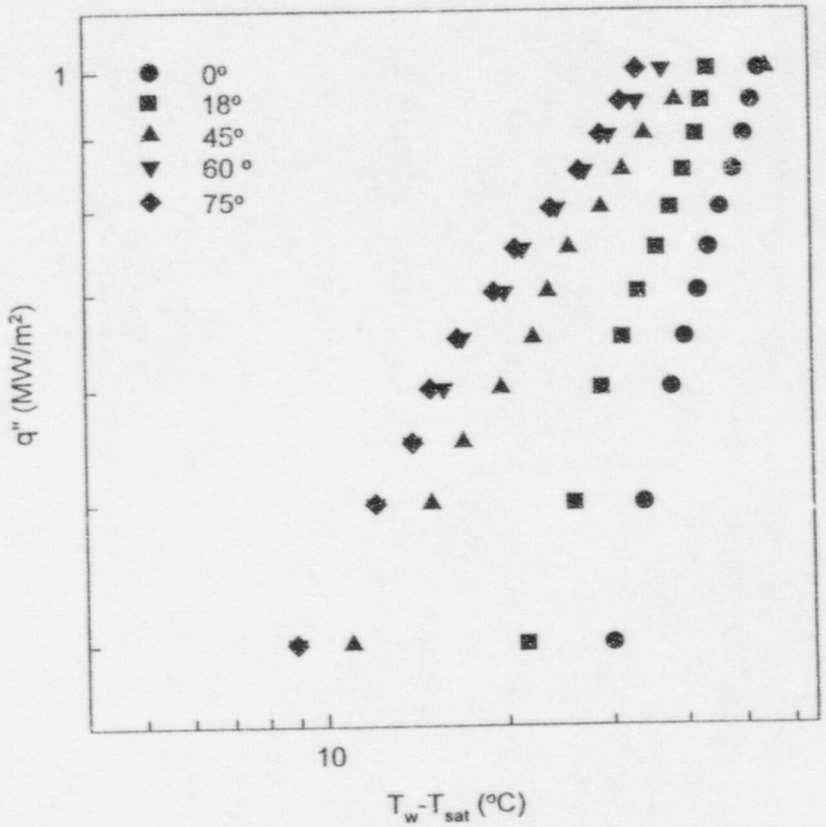

Figure 4.11 Spatial Variation of the Natural Convection Boiling Data Under Saturated Boiling Conditions (T_{water} = 100°C).

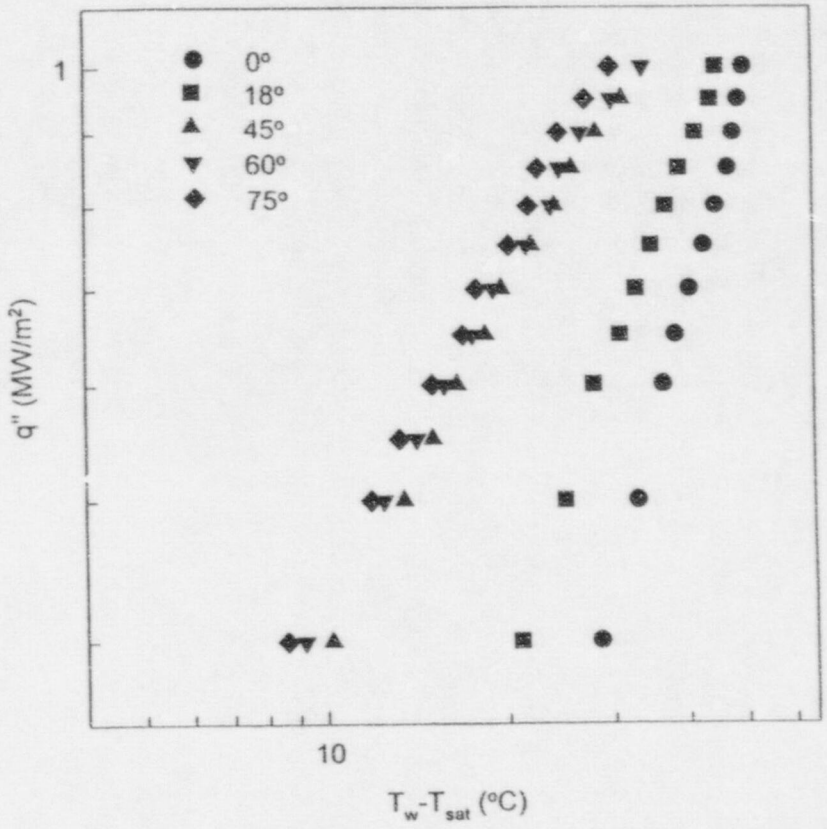

Figure 4.12 Spatial Variation of the Natural Convection Boiling Data Under Subcooled Boiling Conditions (T_{water} = 97°C).

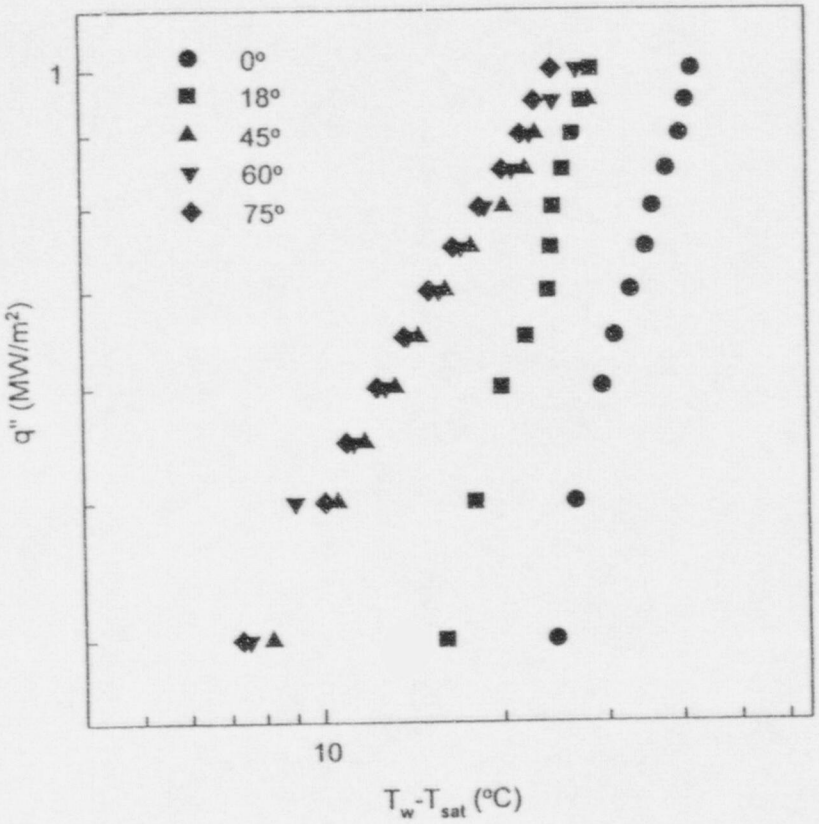

Figure 4.13 Spatial Variation of the Natural Convection Boiling Data Under Subcooled Boiling Conditions (T_{water} = 93°C).

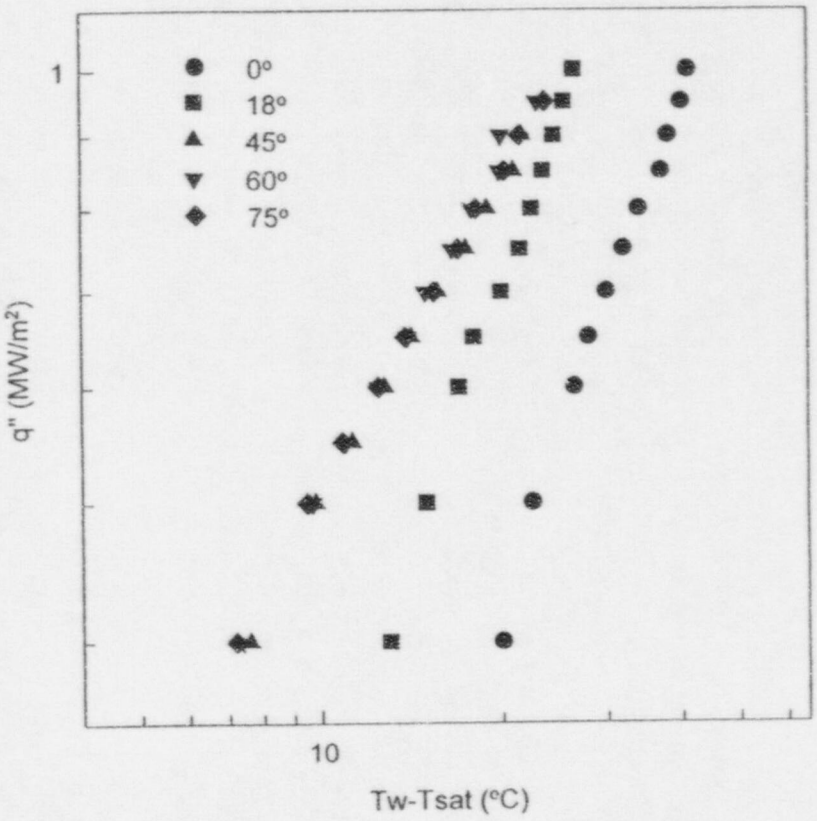

Figure 4.14 Spatial Variation of the Natural Convection Boiling Data Under Subcooled Boiling Conditions (T_{water} = 90°C).

CHF limit was observed in this study with thermal insulation. Local dryout of the wall was not detected at the bottom center of the vessel even for saturated boiling at the heat flux level of 1.10 MW/m^2. As the heat flux was increased to 1.10 MW/m^2, the local wall temperature at the bottom center of the test vessel simply rose to a new steady-state value without showing any abrupt increase in magnitude. This clearly indicated that, with the presence of an insulation structure, the local CHF limit for saturated boiling on the external bottom center of the vessel was larger than 1.10 MW/m^3. This was almost three times higher than the local CHF value of 0.40 MW/m^3 for the case without thermal insulation [3].

Near the minimum gap of the channel ($\theta \sim 45°$), the local CHF limit for saturated boiling was found to be approximately 0.98 MW/m^2. This was considerably lower than the local CHF limit at the external bottom center. Physically, this decrease in the local critical heat flux was evidently due to the difficulty in venting the steam through the minimum gap. As the local CHF limit was approached, the vapor slug tended to occupy the entire cross-sectional flow area at the minimum gap, thus preventing the supply of fresh liquid water to the heating surface. This resulted in a premature dryout of the surface, leading to a considerably smaller value of the local critical heat flux. In view of this, the minimum gap region could be a potential hot spot on the vessel wall under severe accident conditions.

At locations further downstream of the minimum gap, i.e., for $60° \leq \theta \leq 90°$, the local critical heat flux appeared to increase considerably. Even for saturated boiling at the heat flux level of 1.2 MW/m^2, there was no local dryout being detected on the wall. As the heat flux was increased to 1.2 MW/m^2, the local wall temperature simple rose to a new steady-state value without exhibiting any abrupt jump in magnitude, which was similar to the phenomenon observed in the bottom center of the vessel. This confirmed the fact that the local critical heat flux had the lowest limit in the minimum gap region. A comparison of the local CHF values for the cases with and without thermal insulation is given in Table 4.1.

Table 4.1 Local Critical Heat Flux (CHF) for the Cases With and Without Thermal Insulation

Angular Position on the Vessel Outer Surface	0°	18°	45°	60°	75°
Local CHF Value* Without Thermal Insulation, MW/m^2	0.40	0.54	0.74	0.85	0.93
Local CHF Value* With Thermal Insulation, MW/m^2	>1.10**	>1.10**	0.98	>1.20**	>1.20**

* Local CHF value obtained under saturated boiling conditions.

** Local dryout was not observed at the wall for heat fluxes up to the indicated values in MW/m^2.

4.5 Reference

1. Xia, Cl, Hu, W., and Z. Guo, "Natural Convective Boiling In Vertical Rectangular Narrow Channels," *Experimental Thermal and Fluid Science*, Vol. 12, PP. 313-324, 1996.

2. Mishima, K., and Ishii, M. "Flow Regime Transition Criteria for Upward Two-Phase Flow In Vertical Tubes, *Int. J. Heat Mass Transfer*, Vol. 27, No. 5, PP. 723-737, 1984.

3. Cheung, F. B., Haddad, K. H., and Liu, Y. C., "Critical Heat Flux (CHF) Phenomenon on a Downward Facing Curved Surface," NUREG/CR-6507, U. S. Nuclear Regulatory Commission, Washington, D.C., 1997.

4. Cheung, F. B. and Haddad, K. H., "A Hydrodynamic Critical Heat Flux Model for Saturated Pool Boiling on a Downward Facing Curved Heat Surface," *Int. J. Heat Mass Transfer*, Vol. 40, No. 6, PP. 1291-1302, 1997.

5. CONCLUSIONS

Based upon the flow observation and the heat transfer data obtained in this project, the following conclusions can be made:

1. As a result of natural convection boiling on the outer surface of the hemispherical vessel, an upward co-current two-phase flow, driven entirely by buoyancy, was induced in the annular channel between the test vessel and the insulation structure.

2. There were strong upstream influences on the flow field due to the activities of large elongated vapor masses generated by boiling in the external bottom center region of the vessel.

3. At high-heat-flux levels, the two-phase motion in the channel was in the churn turbulent flow regime with flow-induced vibration of the lower octagonal part of the insulation structure.

4. There was a significant spatial variation of the nucleate boiling heat transfer downstream of the bottom center of the vessel. Moreover, a strong effect of subcooling was observed in the entire high-heat-flux region up to the local CHF limit.

5. The rate of steam venting appeared to increase considerably with the power input. Large vapor slugs, occupying the entire cross-sectional flow area, were observed to flow through the minimum gap in a highly unsteady and chaotic manner.

6. Because of the chaotic steam venting process through the minimum gap, the local critical heat flux near the minimum gap was considerably lower than the CHF limit at the bottom center. However, it is still appreciably higher than the corresponding local CHF value for the case without thermal insulation.

Appendix A
Literature Survey

The subject of pool boiling has been extensively reviewed by Cheung et al. [1]. In this appendix, the CHF phenomena for flow boiling will be reviewed.

A.1 CHF In Tubes And Other Circular Geometries

A.1.1 CHF Conditions for Internal Flow Boiling

Internal flow boiling is often encountered in applications where nearly complete vaporization of the coolant is desired. Perhaps the most frequently encountered example is the refrigeration or air-conditioning system. Other examples include cryogenic processing applications, boilers in nuclear and conventional power plant systems, and chemical processing involving pure hydrocarbons. To avoid the occurrence of high wall temperatures and/or the poor heat transfer associated with the film boiling regime, the vaporization must be accomplished at low wall superheat levels. For this reason, evaporators and boilers are usually designed to avoid the high wall superheat levels that may produce film boiling at some point during the process.

Although numerous investigations of critical heat flux conditions for flow boiling have been conducted, the mechanisms responsible for the critical heat flux transition are still not ll understood at the present time. However, some light has been shed on the nature of these mechanisms under subcooled or very low quality conditions, where bubbly or slug flow is typically encountered. For such conditions, three potential mechanisms have been discussed by Tong and Hewitt [2]. These mechanisms are illustrated in Figure A.1.

The first of these mechanism is associated with evaporation of the liquid microlayer under a growing vapor bubble on the heated tube wall (Figure A.1). Just prior to release of the bubble, evaporation of the microlayer may leave a portion of the wall under the bubble completely dry. If a constant-heat-flux condition is applied to the wall, the temperature of the dry patch may rise above the Leidenfrost temperature, preventing the patch from rewetting. Continued evaporation of the microfilm at the perimeter of the dry patch may cause it to grow. This may eventually lead to the dryout of the entire wall, whereupon a transition to convective film boiling occurs.

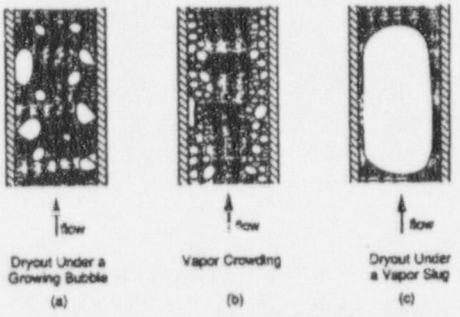

Figure A.1 Schematic Representations of Postulated CHF Mechanisms.

The second mechanism identified by Tong and Hewitt may be encountered at moderate bulk subcooling levels, where bubbles may be concentrated in a boundary layer near the wall. If the number density of the bubbles and size of the bubble boundary layer become large enough, liquid flow to the surface may be impeded. Liquid under and between bubbles at the surface may then be evaporated away, producing dry patches at

the wall. Dry patches produced in this fashion may continue to grow as liquid near the surface is evaporated away, ultimately producing a transition to convective film boiling.

The third mechanism is associated with slug flow encountered for high-quality saturated flows. As a slug moves downstream, the liquid film between the bubble interface and the wall may completely evaporate at a particular location, thus forming a dry patch. For a sufficiently high applied heat flux, the surface temperature may exceed the Leidenfrost temperature and prevent the patch from rewetting. The dry patch may subsequently grow in size, leading to a transition to convective film boiling.

Despite numerous studies of critical heat flux (CHF) conditions, the mechanisms described above are not completely understood. The complexity of these mechanisms has also made analytical modeling generally difficult. As a result, most proposed methods for predicting CHF conditions have been based on experimental data.

In general, for upward flow of water in a round tube, the parameters that may affect the critical heat flux include the mass flux, the pressure, the tube diameter, the location downstream of the tube inlet, and either the quality or subcooling.

The members of the USSR Academy of Sciences [3] reported that critical heat flux increases as the bulk enthalpy of the coolant is increased and decreases as the subcooling is decreased or the quality is increased. For strongly subcooled conditions, increasing the flow rate increases the critical heat flux, apparently because doing so strengthens convective transport. For saturated flow, increasing the mass flux decreases the critical heat flux. When the flow is in the churn or annular regime, this trend is apparently a consequence of the increase in entrainment that generally accompanies increasing mass flux. This is expected because a greater portion of the liquid inventory flows as entrained droplets on the core, making it more difficult to keep the walls fully wetted. At lower heat flux levels, Levitan and Lantsman [4] reported that the critical quality becomes essentially independent of heat flux. The members of USSR Academy of Science reported that increasing mass flux decreases the dryout quality. They attributed this phenomenon to a consequence of increased entrainment, which leaves less liquid in the liquid film on the wall. They also suggest that tubes of larger diameter will have lower critical heat flux values. Doroshchuk et al [5] also presented CHF data at high mass flux levels and suggested that the dryout quality may exhibit some heat flux dependence at very low heat flux levels and high mass flux levels. These investigators attributed this dependence on heat flux to the increased precipitation (deposition) of droplets on the tube wall at higher mass flux levels. This hypothesis was supported by argument that the deposition rate increases as the mass flux is increased.

A.1.2 Non-uniform Heat Flux Distribution of Round Tube

A large amount of data were collected for critical heat flux variation in a tube subjected to axial variation of heating. Keeys et al. [6] reported that the critical heat flux for a tube with a cosine axial heat flux distribution is lower than the critical heat flux at the same local quality with uniform heat flux distribution. The strong effect of heat flux distribution on the local/quality relationship was also observed by Doroschuk et al. [7]. Another form of non-

uniform distribution of heat flux often investigated is that where a short zone in the channel is at a higher flux ("flux spike"). A collection of data and analysis for this case was reported by Greoneveld [8]. The channel average heat flux dryout with a flux spike was found to approach the value for uniform flux as the exit quality increased. In the high quality region, the magnitude of the flux in the flux spike itself can be up to three times the mean flux without changing the average flux for dryout. Similar results were obtained with circumferential variations of heat flux though, here, the average heat flux maybe lower due to limitations of circumferential transport of the liquid; results of this type were presented by Chojonowski [9].

A.2 CHF In Vertical Non-Circular Channels

A.2.1 CHF in Vertical Channels of Reduced Size

Natural convective boiling in a confined narrow space is frequently encountered in various heat transfer equipment. In this case, heat transfer characteristics become quite different from those of conventional unconfined natural convective boiling. In a confined space, opposing effects may arise either to enhance or to degrade heat transfer. Among others, natural convective boiling in narrow vertical channels has become an important problem in many fields of engineering. Cooling of plate-type nuclear fuel elements in nuclear reactors, microelectronic device cooling, where miniaturization and minimization of packaging volume and weight are of paramount importance, and the control of heat transfer properties in various types of heat transfer equipment are just a few examples of the applications motivating research in this area.

Katto and co-workers [10] carried out experiments on nucleate boiling at rather high heat flux in a confined space bounded by two horizontal co-axial disks with the lower disk heated. They classified the boiling behavior depending on the gap size into three regions as: unheated bubbles, depressed bubbles, and oppressed bubbles. They investigated in detail the region of depressed bubbles and pointed out the thin liquid evaporation as a dominant heat transfer mechanism of this region. Ishibashi and Nishikawa [11] performed experiments at rather low heat fluxes in a vertical annuli with both ends open. They identified the isolated bubble region and the coalesced bubble region. Compared with the unconfined situation, the enhanced heat transfer coefficient is attained in the coalesced bubble region and an empirical correlation was proposed for this region. Katto and his co-workers [12-14] developed generalized correlations for the critical heat flux of natural convection boiling in confined spaces, vertical annular channels, and uniformly heated vertical round tubes. Yao and Chang [15] studied pool boiling in a vertical annuli with a closed bottom for various gap sizes, fluids, and heat fluxes. They distinguished three boiling regimes of isolated deformed bubbles, slightly deformed bubbles, and coalesced deformed bubbles, on a boiling map where the Bond number and the boiling number are chosen as the coordinates. Hung and Yao [16] measured the heat transfer coefficient and critical heat flux in a horizontal annuli with open ends, and investigated the effects of annuli length, liquid subcooling, and non-uniform gap due to eccentricity. Fujita et al. [17] and Fujita and Uchida [18] investigated pool boiling heat transfer and critical heat flux for saturated water at atmospheric pressure in a confined narrow channel bounded by opposed heated and unheated parallel rectangular plates. Monde and his

co-workers [19-21] experimentally and theoretically studied heat transfer enhancement due to bubbles passing through a vertical narrow channel with asymmetric heating.

As for the critical heat flux in a confined space, many experiments in vertical channels have been made with cryogenic liquids in relation to superconducting devices. Ogata et al. [22] and Bailey [23] measured the CHF in vertical rectangular channels and proposed an empirical correlation for their own CHF data. Monde et al. [19] performed experiments on critical heat flux in narrow channels submerged in a water pool. In their experiments, the channels were formed by two vertical surfaces. Uniform heating was applied to one surface of the channel, that was submerged in saturated water at one atmosphere. Burnout was detected by observing the temperature excursion in the channel wall. Their data shows that CHF decreases in a roughly hyperbolic fashion with increasing length-to-spacing ratio. As this ratio goes to zero, the CHF data approaches the pool boiling CHF limit. However, as the ratio is increased to 100, the measured CHF is only about one-tenth that of the pool boiling CHF value.

Aritomi et al [24] recently studied the effect of channel gap on thermo-hydraulic behavior at low velocities and atmospheric pressure. Freon 113 was used as the test fluid. The test section was composed of an inner heated rod and an outer tube made of glass. Several findings reported by Aritomi are listed below:

- For channel gaps less than 2 mm, the saturated nucleate boiling heat transfer depends strongly on the gap spacing. On the other hand, for channel gaps larger than 2 mm, the saturated nucleate boiling heat transfer was not influenced by the gap size.

- For channel gaps less than 2 mm, saturated nucleate boiling heat transfer increases with a decrease in the channel gap.

- Boiling heat transfer in the channel gaps larger than 2mm can be evaluated in the same way as those in normal channels, but those in channel gaps <2 mm could not be evaluated by the same correlation.

A quantitative analysis of the critical heat flux in both vertical circular tubes and rectangular channels was carried out by Sudo [25] using the separated two-phase flow model for low-velocity, upward-saturated two-phase flow. Over 1,000 experimental CHF data were compared with the analytical results. Their proposed model was based on an existing model of vapor blanket over the thin liquid sublayer on the heated wall at the CHF point, which was originally proposed by Haramura and Katto [26]. The major findings of their work are listed below:

- The critical heat flux increases with increasing mass flux and inlet subcooling.

- The critical heat flux increases with decreasing channel length.

- The critical heat flux decreases with decreasing gap size.

Xia et al [27] performed experiments using saturated R-113 in vertical narrow channels under atmospheric pressure. The effects of

gap size, channel height, and heat flux on the critical heat flux were studied. The channels consisted of a pair of flat plates. Two different peripheral conditions of the channels were tested. The first was an open periphery where four edges of the confined space were open to the bulk liquid. The second was a closed side periphery with the top and the bottom edges open. Xia et al [27] reported that the smaller the gap size, the smaller the incipient heat flux. For channel spacing greater than 3 mm, the heat transfer data were nearly the same as those for conventional natural convective boiling in a large vertical channel. Their results led to the following conclusions:

- The heat transfer coefficient may increase by a factor of 3 to 5 with a decrease in the channel gap and/or an increase in the channel height at low to moderate heat fluxes (far below CHF). At high heat fluxes, the reverse is true. There exists an optimum channel size for heat transfer enhancement.

- The CHF is reduced with a decrease in the channel gap or an increase in the channel height.

- Because of the complicated boiling heat transfer in the channel, the maximum local superheat point is not always located on the top of the boiling surface.

Furthermore, they found that once the wall heat flux increased to the point where the mass flux reached its maximum, fluid flow began to fluctuate. If the heat flux continued to increase, the mass flux in the channel would fall sharply, and the wall superheat would rise followed by the occurrence of the boiling crisis.

Schoesse et al [28] conducted CHF measurements in a vertical upward annular channel composed of an inner heated rod and an outer tube. The following features were obtained in their investigation:

1. The CHF behavior can be classified into a low mass flow regime, a high mass flux regime, and a transition region.

2. The influence of inlet subcooling on CHF is remarkable only in the transition and high mass flux regions. A minimum CHF is detected under the condition of flow transition from churn to annular flow, located at the exit of the test section.

3. The most probably point of CHF occurrence is related to the region of the most unstable flow conditions. Depending on the influence of mass flux and inlet subcooling, the most unstable flow condition is marked as follow:

    - For low mass fluxes, CHF was induced by the phenomena of flooding and chugging at the top of the heater,

    - For high mass fluxes and high inlet subcoolings, CHF was induced by the pulsated annular flow or churn flow at the top of the heater,

    - For high mass fluxes and low inlet subcoolings, CHF was caused by the churn-annular or bubble-annular flow transition at the middle and lower part of the heater.

It is worthy to note that the above investigations were made for CHF in thin or reduced-size vertical channels. Moreover, none of the previous studies is applicable to the problem under consideration. This is because of the differences in the size of the channel and geometry of the heating surface between the previous studies and present work. Both factors (i.e., the size and the geometry) are expected to have strong effects on the natural convection boiling process. The channel sizes employed in most previous studies were at least an order of magnitude smaller than the size of the hemispherical flow channel considered in the present work.

Recently Rouge [29] performed experiments under forced and natural upward convection conditions in a vertical rectangular channel. The test section was a flat plate, 15 mm thick, 4 m long and 15 cm wide, uniformly electrically heated. Channel width (gap) can be enlarged from 3 to 15 cm, and the test section can be inclined from vertical to horizontal position. The test section was operated under different system conditions:

- Outlet absolute pressure varied from 0.1 to 1 MPa.
- Subcooling varied from 0^0C to 50^0C.
- Heat flux varied from 0.1 to 1 MW/m^2 (with some data up to 2 MW/m^2).

The effects of pressure drop, subcooling, gap size, and inclination were investigated. For a gap width of 0.03m, and inclination of 90^0, they reported that the CHF limit increased when the pressure drop or the mass velocity was increased. There was no influence of subcooling, as the CHF was always observed to occur under saturated conditions. For a gap width of 0.15m, and inclination of 10^0, they reported that the influence of subcooling was much more important than that for the previous case. For near saturation inlet conditions, the influence of mass velocity on the CHF became predominant and at low mass velocities, the CHF curves approached an asymptotic limits (200kW/m^2 at 0.1MPa). Their results indicated favorable possibilities of coolability of large surfaces under natural convection conditions. The major findings of their work are summarized below:

- The critical Heat Flux decreased almost linearly with the quality, with a positive influence of the mass flux at low qualities and a negative influence at high qualities.
- The curves of CHF approached an asymptotic value at large quality.
- The CHF decreased when the inclination was increased.
- The CHF increased slightly when the pressure was increased.
- The channel gap size had no effect on the CHF under saturated conditions in the vertical position, and a limited positive effect under subcooled conditions.

A detailed comparison of previous studies is given in Table A.1 and A.2. Table A.1 summarizes the effects of subcooling and gap size on the CHF limit whereas Table A.2 summarizes the CHF mechanisms under various mass flow and subcooling conditions.

Table A. 1 Effects of Subcooling and Gap Size on the CHF Limit: Comparison of Previous Studies

Source	Heating Geometry	Increased Subcooling on CHF	Increased Gap Size on CHF	Limit
Rouge + [29]	Vertical rectangular channel with one side heated (upward, forced)	No influence	No effect under saturated conditions in the vertical position	Greater than 1 MW/m^2
Rouge + [29]	Same configuration except with 10° degree inclination (upward, forced)	Enhanced	Positive effect under subcooled conditions	Greater than 1 MW/m^2
Schoesse et al. [28]	Vertical annulus (upward, forced)	Enhanced	Not Available	Not defined
Xia et al.* [27]	Vertical rectangular channel with one side heated (upward, natural)	Not considered	Enhanced	Not defined
Sudo [25]	Vertical rectangular channel with both side heated (upward, forced)	Enhanced	Enhanced	Not defined
Monde et al. [19]	Vertical rectangular channel with one side heated (upward, forced)	Not Considered	Enhanced	Greater than 1 MW/m^2

+ The experiments were carried out in vertical channels of large size.
*The test fluids used in the experiments were R-113.

Table A.2 The CHF Mechanism Under Various Mass Flux and Subcooling Conditions: Comparison of Previous Studies

Source	Mass Flux	Subcooling	CHF Mechanism
Schoesse et al. [28]	Low (below 80kg/m^2-s)	No effect	Flooding/flow reversal
	High (higher than 140 kg/m^2-s)	Low	Circulation
		High	Flow reversal
Xia et al. [27]	Low to high	Not Considered	Mass flux sharply drops due to thermal drag
Monde et al. [19]	Low	Not Considered	Flooding/Circulation

A.2.2 Effect of Flow Direction on CHF

Bertonni et al. [30] showed a small reduction in heat flux in going from upflow to downflow. The differences could be accounted for by differences in flow patterns (there is a greater propensity to annular flow in a downward flowing system) and liquid entrainment behavior in downflow as illustrated in the experiments of Webb and Hewitt [31]. Mishima and Nishihara [32] studied the CHF at low-flow-rate and low-pressure conditions for water flowing in thin rectangular channels. Their experiments were carried out with two types of rectangular test sections, namely, the one heated from one wide side and the other heated from two opposite sides. The CHF was measured both in upflow, downflow, and at complete bottom blockage in order to observe the effect of gravity. Their results revealed that the flow regimes under low-flow-rate and low-pressure conditions were significantly affected by the density ratio and gravity. In addition, their results revealed that:

- There was a minimum value in the CHF for the test section heated from one side at complete bottom blockage or low downflow. This minimum occurred due to flooding and/or bubble stagnation. The minimum CHF in downflow appeared at mass velocities up to the critical mass velocity (150 to 200 kg/m^{2}s) at which the bubbles stagnated in the heated section. Beyond the critical mass velocity, the vapor bubbles were forced downward and the flow regime became churn or annular flow accompanied with a violent oscillation of boiling boundary. In this region, the CHF increased as the mass velocity was increased.

- In the upflow, the CHF approached to the minimum due to flooding at the lowest mass velocity, while it increased almost linearly with mass

velocity. It was found that the CHF in upflow was generally higher than in the downflow. The flow characteristics indicated that the effect of gravity was significant at such low flow rates.

- The effect of inlet subcooling on CHF also could be found. In the downflow, the CHF increased with increasing inlet subcooling while in upward flow, the effect was not obvious.

- The general tendencies of the CHF measured in the test section heated on both sides were similar to those observed in the first test section. However, the CHF in the test section heated from two opposite sides was about a half of that in the other test section.

A.3 CHF on External Surfaces

Pool boiling on the underside of inclined and downward-facing curved surfaces is of interest in many applications. Examples include thermal management of ground storage tanks of cryogenic liquids; handling of hazardous liquid chemical containers during a fire (Jung et al. [33]) cooling of high power-density electronics; cooling of electric cables in superconductivity research; and cooling of the pressure vessel lower head of an ALWR following a core meltdown accident involving relocation of a large quality of molten core mixture (corium) to the lower head.

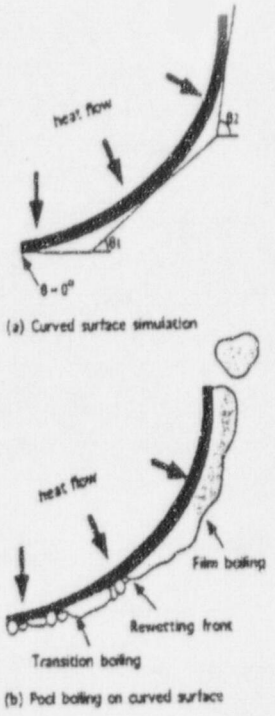

Figure A. 2 Pool Boiling on Curved Surface

Pool boiling on the underside of inclined and downward-facing flat surfaces has also been thought of as a simplified approach for investigating the effect of local inclination on pool boiling on the external surface of a hemispherical or curved wall. The assumption was to neglect the effect of upstream boiling on the curved surface, which has recently been shown not be valid by El-Genk et al [34-36]. Experimental results for flat inclined surfaces showed that nucleate boiling heat flux at high wall superheat increased slightly with increased surface inclination from the horizontal , but decreased significantly with increased inclination at low wall superheat. It was explained that such increase in nucleate boiling heat flux with decreased inclination at low wall superheat could be due to increased mixing in boundary layer by sliding elongated vapor bubbles and to the evaporation of the thin film underneath the bubbles. As the inclination angle of the surface is decreased, the bubbles become

more elongated and their average size and residence time increases, while the thickness of the liquid film underneath the bubbles decreases, resulting in a higher nucleate boiling heat transfer. This dependency of nucleate pool boiling heat flux on local inclination was found to be opposite to those measured for small, downward-facing curved surfaces.

Table A-3 summarizes the local CHF values for downward facing pool boiling reported by various investigators.

A.4 Critical Heat Flux Models For Flow Boiling

A.4.1 Critical Heat Flux Mechanism in Channel Flow

Early attempts to obtain generalized predictions of the critical heat flux for liquids flowing inside a channel were often based on the assumption that the underlying mechanism was essentially the same as the one for pool boiling. Most investigators have now concluded that this is not the case and that the appropriate model depends on the two-phase flow which exists at the CHF limit. It is suggested that there are four flow pattern regions which need to be separately considered. They are:

1. Annular flow: At very high void fractions, a film of liquid normally covers the surface of the heated channel whereas vapor with entrained droplets occupy the central core. The critical heat flux occurs when the liquid film on the heater wall begins to "dry out".

2. Churn-to-annular flow: At high void fractions, the critical heat flux is induced by flooding which results in zero liquid penetration at this point.

Table A. 3 Critical Heat Flux Values Reported by Previous Investigators

Source	Heating Method	Heating Surface	Angle of Inclination	Subcooling Level (K)	Critical Heat Flux (kW/m2)
Theofanous et al. [47]	Steady State Heating	2-D simulation	$0^\circ<\theta<30^\circ$	0	300 if $\theta<5^\circ$ $300+12.6\theta$ if $5^\circ<\theta<30^\circ$ 276 if $\theta<5^\circ$ $276+12.60$ if $5^\circ<\theta<30^\circ$
Theofanous et al. [48]	Steady-State Heating	2-D-full-size simulation	$0^\circ<\theta<15^\circ$ $15^\circ<\theta<90^\circ$	14	$500+13.3\theta$ $540+10.7\theta$
Guo and El-Genk [42]	Quenching	Spherical surface	0°	0	570
Cheung et al. [52]	Quenching	Hemisphere Vessel	$0^\circ<\theta<90^\circ$	0 - 10	400 - 1050
Cheung et al. [1]	Steady-State Heating	3-D Scaled Vessel	$0^\circ<\theta<90^\circ$	0 - 10	$400(1+0.036\Delta T_{sub})$ $[1+0.021\theta-(0.007\theta)^2]$

3. Slug and churn turbulent flows: At medium to high void fractions, these flow patterns are marked by separate vapor and liquid regions and it is possible that the CHF occurs due to overheating during the passage of the vapor clot, dryout of liquid microlayer, or the blockage of the liquid penetration to the microlayer during the heating period.

4. Dispersed bubbly, churn and bubbly flows: The vapor is normally dispersed throughout the liquid but at the CHF point, a film of vapor forms at the wall which then prevents the liquid coolant from contacting the heated surface.

A.4.2 Annular and Churn-to-Annular Flow Regime

A recent review of experimental data on critical heat flux for natural convection boiling in vertical rectangular channels revealed three mechanisms of CHF. They are the pool boiling limit, the circulation limit, and the flooding limit associated with a transition in flow regime from churn-turbulent to annular.

Fujita et al. [17] observed that CHF in thin vertical rectangular channels may be predicted from the limiting condition that the homogeneous flow of a vapor and liquid mixture in a vertical duct, driven by natural circulation, is completely vaporized at the top exit of the heated channel. This burnout mechanism is the circulation-limited burnout that occurs when the flow is low and the vapor quality at the exit approaches unity.

In their study of critical heat flux under conditions of low flow in a vertical annulus, Mishima and Ishii [37] suggested that another mechanism of burnout may result from a transition in flow regime from churn to annular. They observed that this type of burnout occurred over the same range of mass velocity as circulation-limited burnout. The cause of flooding limited burnout is that the liquid from the top is limited by flooding due to high steam flow, resulting in a dryout on the heating surface. For a CHF caused by a transition in flow regime, the steam flow is high enough to prevent liquid flow from the top.

An analytical expression for predicting flooding-limited CHF in thin rectangular channels was recently derived by Cheng [38] from the two-component momentum equations for the liquid and gas phases. Combined with the derivation for circulation-limited and pool-boiling-limited CHF, Cheng [39] was able to predict the CHF of three kinds in rectangular channels.

A.4.3 Slug and Churn Turbulent Flow Regime

Fiori and Bergles [40] observed that the CHF is associated with the passage of vapor plugs. They suggested that the CHF can be reached as a result of the evaporation of the thin liquid layer under the vapor plug during the passage of the plug. In their observation, near the CHF condition, the wall temperature level began to increase and showed temperature fluctuations due to momentary dryout during the vapor passage. These temperature fluctuations grew in amplitude and the temperature level increased rapidly since the temperature rise during the dry period exceeded the temperature drop due to quenching. The cyclical behavior continued until the wall was above the estimated rewetting temperature. Van der Molen and Galijee's [41] more recent photographic observations of the CHF for plug flow in small diameter

vertical annuli lent support to the observations of Fiori and Bergles [40]. The critical heat flux appeared to be associated with the passage of a vapor plug. These investigators found that in the intermittent flow pattern there were large variations in the time average temperature around the circumference of the evaporator tube. They concluded that the vapor regions traveling along the upper wall act as barriers and inhibit coolant contact with the top wall. With a sufficiently high heat flux, one might expect the temperature of the upper surface to reach a point where rewetting is no longer possible.

It should be noted that currently there is no successful theoretically based predictive model accounting for the observation that the CHF arises from vapor plug passage. Development of such CHF predictive capability will require a model of the intermittent flow pattern which can accurately predict the length of the vapor region, the interval between vapor region and vapor region passage time.

Recently Ho et al. [42] developed a theoretical critical heat flux model for low-pressure, low mass, and low-steam-quality flow conditions. They assumed that the occurrence of CHF under such conditions was triggered by Helmholtz instability in the sublayer stem-liquid system. Their model was developed by a simple energy balance of liquid sublayer evaporation as the vapor blanket tended to disturb the balance between the buoyancy force and the drag force exerted upon it. The result showed good agreement with experimental data.

A.4.4 Bubbly, Churn-Bubbly Flow

Under the conditions of subcooled and low quality flow, the flow pattern is expected to be bubbly, churn and bubbly flow. The major theoretical approaches to CHF in this situation have focused on the very thin liquid layer between the wall and the bubbly layer. Katto [43] suggested that the major theoretical approaches to CHF can be categorized into the following groups:

1. Critical liquid superheat: CHF is assumed to occur when the thin liquid sublayer (beneath the bubbly layer) reaches a critical superheat.

2. Inhibition of enthalpy transport to the bubbly layer due to separation of the boundary layer from the wall.

3. Blockage of the liquid flow to the wall by the flow of vapor from the wall.

4. Dryout of the liquid sublayer underneath vapor clots flowing along the wall.

5. Bubble coalescence in the bubbly layer brought about by inadequate vapor removal rate at the edge of the bubbly layer.

Among these groups, only the liquid dryout and the bubbly coalescence theories are receiving significant attention. Hebel et at. [44] assumed that limitation for the rate of the vapor removal by axial transport of vapor leads to the shortage of liquid, resulting in the occurrence of CHF. Weisman and co-workers [45] considered a critical value of void fraction in the bubble layer adjacent to the wall, which is brought about through the balance between the outward flow of vapor bubbles and the inward flow of liquid at the bubble-layer/bulk-flow interface. Their CHF model which employed two-empirical constants gave good predictions for various kinds of liquids under slightly subcooled and low quality conditions.

The CHF modeling based on dryout of a liquid sublayer under vapor clots was originated by Lee and Mudawar [46]. The onset of CHF was explained in terms of the dryout of a very thin liquid sublayer which lies below the thin vapor layer at DNB (Departure from Nucleate Boiling). Helmholtz instability was assumed to govern the release of the vapor clot. Hence, the length of the vapor clot was assumed equal to the Helmholtz critical wavelength. The liquid mass flux was simply obtained from the product of bubble velocity and density, where the bubble velocity was determined by a balance of the buoyancy and drag forces acting on the vapor. The sublayer thickness was based on a force balance on the vapor clot in the radial direction. The rate of momentum produced by sublayer evaporation into the vapor was balanced by a lateral force caused by the rotation of the blanket due to the relative velocity between the two phase. Their model which employed a constant and a coefficient, both determined empirically, was shown to predict the CHF of water fairly well over a considerably wide range of subcooling.

A.5 Review of Relevant Two-Phase-Flow Models

Developments of the full governing equations for three-dimensional, time-varying two-phase flow can be found in the works of Ishii [47] and Boure [48]. The form of the governing equations can be simplified by invoking time and/or space averaging. In doing so, however, information regarding the instantaneous localized behavior of the flow is lost. In Carey's [49] treatment of internal gas-liquid flows, the flow was considered to be steady and one-dimensional in the sense that all dependent variables are idealized as being constant over any cross section of the tube or duct, varying only in the axial direction.

By invoking the laws of conservation of mass and momentum for a stratified flow, Carey [49] was able to derive a final expression for the overall pressure gradient for two-phase flow in a channel. There are four contributions to the overall pressure gradient. The first represents pressure variations due to changes in the cross-sectional area of the duct. The second and the third account for frictional and gravitational head loss, respectively, and the forth represents acceleration (or deceleration) of the flow. Carey further developed this one-dimensional model of momentum transport under the following assumptions:

1. At a given axial location in the channel, the velocities of the liquid and vapor phases are uniform over the portion of the channel occupied by each, but not necessarily equal.

2. The two phases are in local thermodynamic equilibrium.

3. Empirical correlations or relations derived from simplified theories are available to predict the void fraction α and one of these two-phase multipliers φ_l, φ_{lo}, and φ_v from parameters that quantify the local conditions. The two-phase multipliers mentioned above are defined as

$$\phi_l = \left[\frac{(dP/dz)_{fr}}{(dP/dz)_l} \right]^{1/2} \qquad \textbf{(2.1)}$$

$$\phi_{lo} = \left[\frac{(dP/dz)_{fr}}{(dP/dz)_{lo}} \right]^{1/2} \qquad \textbf{(2.2)}$$

$$\phi_v = \left[\frac{(dP/dz)_{fr}}{(dP/dz)_v}\right]^{1/2} \qquad (2.3)$$

In the above expressions, *fr* denotes the frictional component of the two-phase pressure drop, *l* the frictional pressure gradient that would result if the liquid flowed alone through the channel at a mass flow rate equal to *G(1-x)A*, *lo* the frictional pressure gradient that would result if liquid only flows through the channel at the same total mass flow rate *GA*, and *v* the frictional pressure gradient that would result if the vapor flowed alone through the channel at a mass flow rate equal to *GxA*.

A.5.1 Analytical Models of One Dimensional Two-Phase Flow

During convective vaporization and condensation processes inside tubes, the large difference between the liquid and vapor densities away from the critical point can result in high vapor void fractions even at relatively low quality. Therefore, this would very likely correspond to the annular flow regime with a thin film of liquid flowing along the tube walls.

The importance of annular flow to air-conditioning systems and other applications has stimulated efforts to develop accurate methods to predict the transport in such circumstances. In this section, analytical treatments of annular flow are briefly presented.

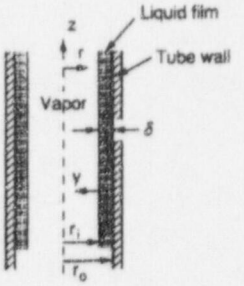

Figure A. 3 Idealized Model System Used in the Analysis of Annular flow without Entrainment

There are four assumptions made by Carey [49] in the analysis of annular flow in a vertical round tube. They are: (1) the flow is steady, (2) the downstream pressure gradients felt in the core and the liquid film are the same, (3) the liquid flows in an annular film on the inside wall of the tube that has a uniform thickness and a smooth liquid-vapor interface, and (4) there is no entrainment of liquid film in the core. Carey argued that the effects of the wavy interface on heat transfer and pressure drop are often small or can be treated by empirically modifying a smooth-interface model.

As shown by Hewitt and Hall-Taylor [50], the streamwise force-momentum balance for the vapor core flow can be expressed as

$$\frac{dP}{dz} = -\frac{4\tau_i}{d_i} - \frac{2xG^2}{\alpha^2\rho_v}\left(\frac{dx}{dz}\right) - \rho_v g \qquad (2.4)$$

The momentum equation for the liquid film with the assumptions of steady-state and neglecting inertia effects requires that

$$\tau(r) = \tau_i\left(\frac{r_i}{r}\right) + \frac{1}{2}\left(\frac{dP}{dz} + \rho_l g\right)\left(\frac{r_i^2 - r^2}{r}\right) \qquad (2.5)$$

where $r_i = d_i/2$ is the radius of the tube.

Also the conservation of mass gives

$$\left(\frac{d_i^2}{4}\right)G(1-x)=\rho_l\int_0^{\delta}u(d_i-2y)dy \qquad (2.6)$$

The conservation of energy (neglecting sensible cooling of the film) also requires that

$$\frac{dx}{dz}=\frac{4q^{"}}{Gd_ih_{lv}} \qquad (2.7)$$

The boundary conditions for the liquid film are

at y=0 $\qquad u=0 \qquad (2.8)$

at y=δ $\qquad \frac{du}{dy}=\frac{\tau_i}{\mu_l+\varepsilon\rho_l} \qquad (2.9)$

For specified values of $q"$, G, x, d_i, and fluid properties, the above differential equations with the boundary conditions can be solved for the velocity profile in the film only if relations are available to determine (dP/dz), τ_i, ε, and δ simultaneously. Therefore two additional relations are required to close the system of equations mathematically. Closure of the system is usually achieved by including empirical relations for determining the interfacial shear stress and the eddy diffusivity. Wallis [51] proposed a simple correlation to determine the interfacial shear stress in terms of an interfacial friction factor f_i, defined as

$$\tau_i=\frac{f_iG^2x^2}{2\rho_v\alpha^2} \qquad (2.10)$$

$$f_i=0.005\left(1+300\frac{\delta}{d_e}\right) \qquad (2.11)$$

The eddy diffusivity in the liquid film for turbulent flow conditions has typically been evaluated using relations like those developed for single-phase turbulent flow in tubes. The Deissler correlation is one of these relations:

$$\varepsilon=n^2u_*y\left(1-e^{-\rho_l n^2u_*y/\mu_l}\right) \qquad (2.12)$$

where n is a constant equal to 0.1.

A.5.2 Empirical Methods for Pressure Drop and Void Fraction

In order to close the system of equations for the separated flow analysis, one needs to determine the two-phase multiplier and void fraction. The methodologies developed to predict these quantities have been typically based on a combination of semi-theoretical arguments and empirical evidence. The most pioneering work was done by Martinelli and his co-worker in the 1940s. They provided the first widely accepted and successful methods for predicting these quantities, and established an analytical foundation on which much of the subsequent work on the two-phase flow has been built.

Lockhart and Martinelli's correlation [52] was based on data from a series of studies of adiabatic two-phase flow in horizontal tubes. The relations used to predict ϕ_l and ϕ_v are

$$\phi_v=\left(1+CX+X^2\right)^{1/2} \qquad (2.13)$$

$$\phi_l=\left(1+\frac{C}{X}+\frac{1}{X^2}\right)^{1/2} \qquad (2.14)$$

The constant C is based on the flow regimes associated with the flow of the vapor and the liquid alone in the duct. The constants associated with each of the four possible combinations are given in Table A.4. In addition, Chisholm &Laird [53] proposed a

correlation that is used by most researchers for two-phase flow in a channel. When the flow of the liquid phase and the gas phase alone is turbulent, the two-phase flow multiplier ϕ_l can be expressed as

$$\phi_l = \left(1 + \frac{21}{X} + \frac{1}{X^2}\right) \qquad \textbf{(2.15)}$$

Wallis [51] also proposed a separate cylinder model for predicting ϕ_l and ϕ_v. An actual two-phase flow is taken to be equivalent to the model flow circumstances in which the vapor and liquid phases flow at the same flow rates through separate cylinders. The final expressions for the two-phase multipliers are

$$\phi_l^2 = \left[1 + \left(\frac{1}{X}\right)^{4/(5-n)}\right]^{(5-n)/4} \qquad \textbf{(2.16)}$$

$$\phi_v = \left[1 + X^{4/(5-n)}\right]^{(5-n)/4} \qquad \textbf{(2.17)}$$

If the flows associated with the two phase are both turbulent, then the value of n is 0.25 for a round tube. Equation (2.16) reduces to

$$\phi_l^2 = \left[1 + \left(\frac{1}{X_n}\right)^{16/19}\right]^{19/8} \qquad \textbf{(2.18)}$$

The definition of Martinelli parameter for turbulent flow on both phases, X_n, is given by

$$X_n = \left(\frac{\rho_v}{\rho_l}\right)^{0.5}\left(\frac{\mu_l}{\mu_v}\right)^{0.125}\left(\frac{1-x}{x}\right)^{0.875} \qquad \textbf{(2.19)}$$

The relation between ϕ_{lo} and ϕ_l can be easily shown to be

$$\phi_{lo}^2 = \phi_l^2 (1-x)^{1.75} \qquad \textbf{(2.20)}$$

A method for predicting the void fraction is essential for predicting the acceleration and gravitational head loss components of the pressure gradient in two-phase flows. Butterworth [53] has shown that several of the available void-fraction correlations can be cast in the following form:

$$\alpha = \left[1 + A\left(\frac{1-x}{x}\right)^a\left(\frac{\rho_v}{\rho_l}\right)^b\left(\frac{\mu_l}{\mu_v}\right)^c\right]^{-1} \qquad \textbf{(2.21)}$$

where the values of the unspecified constants in this relation corresponding to different correlations reported by Wallis [51], Lockhart and Martinelli [52], Thom [54], Barcozy [55] and Zivi [56] are listed in Table A.5.

For engineering design calculations, selection of a two-phase flow model should be done carefully. Carey [49] argued that the homogeneous model yielded reasonably

Table A. 4 Constants used in the Lockhart and Martinelli Correlation.

Liquid	Gas	Subscripts	C
Turbulent	Turbulent	Tt	20
Viscous	Turbulent	Vt	12
Turbulent	Viscous	Tv	10
Viscous	Viscous	Vv	5

accurate results only for limited circumstances. The best agreement was expected for bubbly or dispersed droplet flow, where the slip velocity between the phases was small. Martinelli and Nelson's [57] correlation has been shown to yield reasonable accurate results for a wide variety of two-phase flow circumstances in round tubes and simple channel geometries. This correlation has also been adapted to fit data for complex finned channel and coil geometries. Given the data base from which this correlation was derived, it is expected to yield best results at low pressures for adiabatic or boiling flows at low heat flux levels. As with most correlations of this type, the proposed correlation method neglects the possible effects of the following factors: (1) flow regime; (2) inclination of the channel; (3) rate of the change of quality with length due to evaporation or condensation.

Zuber [58] proposed a void fraction correlation for low-to-high mass fluxes under subcooled conditions based on the drift-flux model. He argued that at low mass flow rates the net of vapor generation was determined by thermal conditions, whereas at high mass flow rates it depended upon hydrodynamic conditions. Simple criteria could be derived which could be used to predict the value of the equilibrium quality at the point of net vapor generation. These criteria were then used to determine the vapor void fraction in subcooled boiling. Comparison between the results predicted by his analysis and experimental data showed good agreement for a wide range of operating conditions, fluids, and geometries. The void fraction can be expressed as:

$$\alpha = \frac{X_t}{C_0\left[X_t + \frac{\rho_g}{\rho_l}(1 - X_t)\right] + \rho_g U_{gj} / G} \qquad \textbf{(2.22)}$$

$$X_t = \frac{X_{eq} - X_d \exp\left(\frac{X_{eq}}{X_d} - 1\right)}{1 - X_d \exp\left(\frac{X_{eq}}{X_d} - 1\right)} \qquad \textbf{(2.23)}$$

$$X_d = -0.0022\left(\frac{q_{CHF}}{\rho_l h_{fg}}\right)\left[\frac{D}{k_l / (C_{pl}\rho_l)}\right] \qquad \textbf{(2.24)}$$

$$C_0 = 1.13 \qquad \textbf{(2.25)}$$

Table A. 5 Constants used in Various Correlations for Void Fraction

Correlation or Model	A	A	B	c
Wallis [52] separate-cylinder model	1	0.72	0.4	0.08
Lockhart and Martinelli Correlation [53]	0.28	0.64	0.36	0.07
Thom correlation [55]	1	1	0.89	0.18
Baroczy correlation [56]	1	0.74	0.65	0.13
Zivi model [57]	1	1	0.67	0

$$U_{gi} = 1.41\left(\frac{\sigma g \Delta\rho}{\rho_l^2}\right) \quad (2.26)$$

$$X_{eq} = (h_l - h_{sat})/h_{fg} \quad (2.27)$$

Sadatomi and Sato [59] investigated the two-phase frictional pressure drop in vertical noncircular channels: rectangular, isosceles-triangular and concentric annular. They proposed a friction factor for a channel with a smooth wall in the turbulent flow regime by the following power-law equation similar to Blausius:

$$f = C_t \mathrm{Re}^{-0.25}$$

The coefficient C_t alone represented channel geometry and was termed as geometry factor for turbulent flow by the authors. With a series of measurements of the pressure drops for non-circular channels, they proposed a correlation for f, which is given by

$$\frac{C_t}{C_{to}} = \sqrt{\left(0.0154\frac{C_l}{C_{lo}} - 0.012\right) + 0.85} \quad (2.29)$$

In the above equation C_{lo} has a value of 64 based on the coefficient for friction factor for the laminar flow regime. For a given channel geometry, C_t can be estimated from the above equation once C_l is obtained either from the available data in the literature or from a numerical calculation. Then the friction factor for turbulent flow can be determined. The frictional pressure drop in noncircular channels can be predicted by using the two-phase multiplier proposed by Chisholm & Laird [53].

A.5.3 Two-Phase Pressure Drop and Void Fraction in Other Geometries

In the above section, the two-phase pressure drops are correlated for vertically and horizontally straight tubes with the use of Lockhart-Martinelli parameters. The questions raised here are how these correlations apply for curved or inclined tubes, or how the inclination and geometry affect the accuracy of these correlations.

Rippel et al. [60] worked on the two-phase flow of gas and liquid in a helicoidal tube with an inside diameter of 12.7 mm and a coil diameter of 208 mm. The working fluids were air-water, helium-water, Freon-12-water and air-2-propanol. They found that their data can be correlated fairly well with values of about 40% precision. Owhadi et al. [61] also found satisfactory agreement between their two-phase flow pressure drops in a helical coil and Lockhart-Martinelli correlation using a modified Lockhart-Martinelli parameter. Comprehensive research on two-phase flow in a coil was reported by Banerjee et al. [62]. The Lockhart-Martinelli correlation was slightly modified and was found to correlate the data satisfactorily. The helix angle, if small, appears to have no discernible effect on the pressure drop.

Boyce et al. [63] found that the Lockhart-Martinelli correlation [52] adequately predicted the data. However, Akagawa et al. [64] found that the frictional pressure drop of two-phase flow in helical tubes is 10 to 50 % larger than that in a straight pipe over their experimental range. Three types of empirical equations for the frictional pressure drop were proposed and also the experimental data were correlated by a modified Lockhart-Martinelli approach independent of the tube diameter to coil diameter ratio. Kasturi and Stepanek [65] used air-water, air-corn-sugar-water, air-glycerol-water and air-butanol-water solutions in their experiments to measure the pressure drop. The data were compared with the Lockhart-Martinelli correlation [52] and

Dukler's correlation [66]. They found that the Lockhart-Martinelli correlation conformed to the data better than Dukler's correlation, but there was a systematic displacement of the curves for various systems in the Lockhart-Martinelli plot. In their continued study (Kasturi and Stepanek, [67]), the correlations for the pressure drop were reported in terms of new correlating parameters that consisted of a combination of known dimensionless groups obtained using the separate flow model.

In the work of Rangacharyulu and Davies [68], a new correlation for two-phase flow frictional pressure drop was proposed based on a modified extension of the Lockhart-Martinelli theory. The experimental data are well correlated in terms of dimensional groups other than the Lockhart-Martinelli parameter. Chen and Zhou [69] found that the major factors affecting the two-phase friction factor are the gas fraction, liquid Reynolds number, gas Reynolds number and the tube to coil diameter ratios. Mujawar and Rao [70] pointed out that the two-phase flow pressure drop can be successfully correlated by the Lockhart-Martinelli method if the flow patterns are specified. Hart et al. [71] reported experimentally that the axial pressure drop of two-phase flow in a helicoidal tube increased as a function of the volume flow rate of the gas, but no attempt was made to correlate the data. Recently, Saxena et al. [72] proposed a method to correlate the pressure drop data for two-phase flow in a helicoidal tube, by retaining the identity of each phase and separately accounting for the effects of curvature and tube inclination resulting from the torsion of the tube.

In summary, for two-phase flow in vertical helicoidal tubes, the Lockhart-Martinelli method is suitable for correlating the pressure drop data under certain conditions. By introducing some newly defined or modified Lockhart-Martinelli parameters, they can predict the two-phase pressure drop quite well. Although Martinelli's correlation was specifically derived for horizontal flows without phase change or significant acceleration, it is often used to calculated both the void fraction and frictional pressure drop for two-phase flow with other effects. This procedure leads to progressively increasing errors as the frictional component of pressure drop decreases in proportion to the other terms.

A.5.4 Flow Regime Transition Criteria for Upward Two-phase Flow in Vertical Tubes

In analyzing two-phase flow transients such as in nuclear reactors under severe accident conditions, a two-fluids model is often required because of its detailed description of thermodynamic transients and phase interactions. The main difficulties in modeling arise from the existence of interfaces between phases and discontinuities associated with them. The internal structures of a two-phase flow are classified by the flow regimes or flow patterns. Various transfer mechanisms between two-phase mixture and the wall, as well as between the two phases, depend on the flow regimes. This leads to the use of regime dependent correlations together with two-phase flow regime maps.

Traditionally, flow regimes are identified from a flow-regime map obtained from experimental observations. Many flow regime maps have been proposed using dimensional coordinates based on the liquid and gas superficial velocities. There have also been theoretical works to predict flow regimes. These conventional flow-regime maps are based primarily on the liquid and gas superficial velocities or the total mass

velocity and quality. However, Mishima and Ishii [73] argued that flow regimes are the classifications of geometrical structures of flow which should depend directly on the geometrical parameter such as the void fraction and interfacial area. They further argued that these traditional approaches may be suitable for slow transients and near fully developed conditions. However, they could fail near flow reversal conditions or under rapid transient conditions. In view of these, new flow-regime criteria for upward gas-liquid flow in vertical tubes were proposed by Mishima and Ishii [73]. The criterion for bubbly-to slug flow transition is given by

$$\alpha = 0.3 \tag{2.30}$$

The transition criterion for the slug to churn-flow transition is given by

$$\alpha \geq 1 - 0.813\left[(C_0 - 1)j + 0.35\sqrt{\Delta\rho g D/\rho_l}\right]^{0.75} \times \left\{j + 0.75\sqrt{\Delta\rho g D/\rho_l}\left[\Delta\rho g D^3/(\rho_l \nu_l^2)\right]^{1/18}\right\}^{0.75} \tag{2.31}$$

where

$$\alpha = j_g / \left[C_0 j + 0.35\sqrt{\Delta\rho g D/\rho_l}\right] \tag{2.32}$$

In the above expression, it is assumed that the transition from the slug-to-churn flow-regime occurs when the mean void fraction over the entire region reaches the mean void fraction in the slug-bubble section.

There are two mechanisms postulated accounting for the transition from churn-to-annular flow regime: (a) flow reversal in the liquid film section along large bubbles, and (b) destruction of liquid slugs or large waves by entrainment or deformation. The transition criterion for churn to annular flow was developed by postulating flow reversal in the liquid film along large bubbles. It is given by

$$j_g \geq \sqrt{\Delta\rho g D/\rho_l}(\alpha - 0.11) \tag{2.33}$$

where the void fraction is given by;

$$\alpha = j_g / \left[C_0 j + \sqrt{2}\left(\sigma g \Delta\rho/\rho_l^2\right)^{1/4}\right] \tag{2.34}$$

The transition criterion for the annular-mist flow is

$$j_g \geq \left(\sigma g \Delta\rho/\rho_g^2\right)^{1/4} N_\mu^{-0.2} \tag{2.35}$$

where

$$N_\mu = \mu_l / \left[\rho_l \sigma \sqrt{\sigma/(g\Delta\rho)}\right]^{1/2} \tag{2.36}$$

The value of C_o is given by

$$C_0 = 1.2 - 0.2\sqrt{\left(\frac{\rho_g}{\rho_l}\right)} \tag{2.37}$$

for round tubes and

$$C_0 = 1.35 - 0.35\sqrt{\left(\frac{\rho_g}{\rho_l}\right)} \tag{2.38}$$

for rectangular ducts.

The above criteria have been compared with the conventional criteria and experimental data for atmospheric pressure air-water flows and high pressure steam-water flows in round tubes and rectangular channels under steady-state and fully developed flow conditions. They reported that there existed wide discrepancies among the experimental data, not only due to the different methods of observations of the flow regimes but also

due to the transition phenomena themselves which develop gradually. However, when these factors were accounted for, it could be said that the criteria showed satisfactory agreements with the data.

A.6 References

1. Cheung, F. B., Haddad, K. H., and Liu, Y. C., "Critical Heat Flux Phenomenon on a Downward Facing Curved Surface", NUREG/ CR – 6507, June, 1997.

2. Tong, L. S., Hewitt, G. F., "Overall Viewpoint Of Flow Boiling CHF Mechanisms", ASME Paper 72-HT-54, Presented at the National Heat Transfer Conf., 1972.

3. Heat and Mass Transfer Section, Scientific Council, *USSR Academy of Sciences*, "Tabular Data for Calculating Burnout When Boiling Water In Uniformly Heated Round Tubes", Thermal Eng. (USSR), English Transl., Vol. 23, No. 9, PP. 90-92, 1976.

4. Letivan, L. L., and Lantsman, F. P., "Investigating Burnout With Flow of a Steam-Water Mixture in a Round Tube", Thermal Eng. (USSR), English Trans., Vol. 22, No. 1, PP. 102-105, 1975.

5. Doroshchuk, V.E., and Lantsman, F. P., "Selecting Magnitudes of Critical Heat Fluxes with Water Boiling in Vertical Uniformly Heated Tubes", *Thermal Eng.* (USSR), English Transl., Vol. 17, No. 12, PP. 18-21, 1970.

6. Keeys, R. K. F., Ralph, J. C. and Roberts, D. N., "Post Burnout Heat Transfer in High Pressure Steam-Water Mixtures in a Tube with Cosine Heat Flux Distribution", *UKAEA Report No.* AERE-R6411, *Published in Progress in Heat and Mass Transfer*, Vol. 6, PP. 99-118, 1972.

7. Doroschuk, V. E., Levitan, L. L., Lantzman, E. P., Nigmatulin, R. I. and Borevsky, L. Y., "Investigations into Burnout Mechanism In Steam-Generating Tubes", Paper to be presented at the *6th International Heat Transfer Conference*, Tokyo, Aug. 1978.

8. Groeneveld, D. C., "The Effect of Short Flux Spikes on the Dryout Power", *AECL* Report No. AECL-4927 1975.

9. Chojnowski, B. and Wilson, P. W., "Critical Heat Flux for Large Diameter Steam Generating Tubes with Circumferentially Variable and Uniform Heating", *Heat Transfer*, Vol. 4, Scripta Book Co., PP. 260-264, 1974.

10. Katto, Y., and Yokoya, S., "Experimental Study of Nucleate Pool Boiling in Case of Making Interference-Plate Approach to the Heating Surface", Proceeding of 3rd Int. Heat Transfer Conference, Vol. 3, PP. 219-227, 1966.

11. Ishibashi, E., and Nishikawa, K., "Saturated Boiling Heat Transfer in Narrow Spaces", *Int. J. Heat Mass Transfer* Vol. 12, pp. 863-894, 1969.

12. Katto, Y., "Generalized Correlation for Critical Heat Flux of Natural Convection Boiling in Confined Channels", *Transactions of JSME*, Vol. 44, PP. 3908-3922, 1978.

13. Katto, Y., and Kurosaka, T., "Critical Heat Flux of Natural Convection Boiling in Vertical Annular Channels", *15th National Heat Transfer Symposium of Japan*, PP. 280-282, 1979.

14. Kawamura, S., and Katto, Y., "Critical Heat Flux of Natural Convection Boiling in Vertical Uniformly Heated Round Tubes", 16th National Heat Transfer Symposium of Japan, PP. 280-282, 1980.

15. Yao, S. C., and Chang, Y., "Pool Boiling Heat Transfer in a Confined Space", Int. J. Heat Mass Transfer, Vol. 26, PP. 841-848, 1983.

16. Hung, Y. H., and Yao, S. C., "Pool Boiling Heat Transfer in Narrow Horizontal Annular Surfaces", J. Heat Transfer, Vol. 107, PP. 656-662, 1985.

17. Fujita, Y., Ohta, H., Uchida, S., and Nishikawa, K., "Nucleate Boiling Heat Transfer and Critical Heat Flux in Narrow Space Between Rectangular Surfaces", *Int. J. Heat Mass Transfer*, Vol. 3, No. 2, PP. 229-239, 1988.

18. Fujita, Y., and Uchida S., "Boiling Heat Transfer and Critical Heat Flux in a Confined Narrow Space", *Proc. 9th Int. Heat Transfer Conference*, Hemisphere Publishing Corporation, New York, 1990.

19. Monde, M., Kusuda, H., and Uehara, H., "Critical Heat Flux During Natural Convective Boiling in Vertical Rectangular Channels Submerged in Saturated Liquid", *Transaction of the ASME*, Vol. 104, PP. 300-303, 1982.

20. Monde, M., "Characteristics of Heat Transfer Enhancement Due to Bubbles Passing through a Narrow Vertical Channel", J. Heat Transfer, Vol. 110, PP. 1016-1019, 1988.

21. Monde, M., and Mitsutake, Y., "Enhancement of Heat Transfer Due to Bubbles Passing through a Narrow Vertical Rectangular Channel", *Int. J. Multiphase Flow*, Vol. 15, PP. 803-814, 1989.

22. Ogata, H., et al., "Boiling Heat Transfer of Liquid Helium in Long Narrow Channels", *Cryogenic Engineering*, Vol. 4, No. 5, PP. 219-225, 1969.

23. Bailey, R. L., "Heat Transfer to Liquid Helium Design Data for Both Cooled Super Conducting Magnets", *Prog. of the 5th International Conference on Magnet Technology*, PP. 582-589, 1975.

24. Aritomi, M., Miyata, M., Horiguchi, M., and Sudi, A., "Thermal-Hydraulics of Boiling Two-Phase Flow in High Conversion Light Water Reactors (Thermo-Hydraulics at Low Velocities)", Int. J. Multiphase Flow Vol. 19, No. 1, PP. 51-63, 1993.

25. Sudo, Y., "Critical Heat Flux of Comparatively Low-Velocity Upward-Saturated Two-Phase Flow in Vertical Channels", Heat Transfer-Japanese, 23(8), PP. 739-755, 1994.

26. Haramura, Y., and Katto, Y., "A New Hydrodynamic Model of the Critical Heat Flux, Applicable Widely to Both Pool and Forced Convective Boiling on Submerged Bodies in Saturated Liquids", *Int. J. Heat Mass Transfer*, Vol. 26, PP. 389-399, 1983.

27. Xia, C., Hu, W., and Guo, Z., "Natural Convective Boiling in Vertical Rectangular Narrow Channels", Experimental Thermal and Fluid Science, Vol. 12, PP. 313-324, 1996.

28. Schoesse, T., Aritomi, M., Kataoka, Y., Lee, S.-R., Yoshioka, Y , and Chung, M. K., "Critical Heat Flux in a Vertical Annulus Under Low Upward Flow and

Near Atmospheric Pressure", *J. of Nuclear Science and Tech.*, Vol. 34, No. 6, PP. 559-570, June, 1997.

29. Rouge, S., "Sultan Test Facility Large Scale Vessel Coolability in Natural Convection at Low Pressure", Workshop on In-vessel core debris retention and coolability, Garching, Germany, March 3-6, 1998.

30. Bertoni, R., Cipriani, and R., Cumo, M., "Upflow and Downflow Burnout", *CNEN Report No. CNEN/RT/ING(76)24*, 1976.

31. Webb, D. R., and Hewitt, G. F., "Downwards Concurrent Annular Flow", *Int. J. Multiphase Flow*, Vol. 2, No 1, PP. 35-49, June 1975.

32. Mishima, K., and Nishihara, H., "The Effect of Flow Direction and Magnitude on CHF for Low Pressure Water in Thin Rectangular Channels", *Nuclear Engineering and Design* Vol. 86, PP. 165-181, 1985.

33. Jung, D. S., Venart, E. S., and Sousa, A. C. M., "Effects of Enhanced Surfaces and Surface Orientation on Nucleate and Film Boiling Heat Transfer in R-11", *Int. J. Heat Mass Transfer.*, Vol. 30, PP. 2627-2639, 1987.

34. El-Genk, M. S., Glebov, A. G., and Guo, Z., "Pool Boiling from Downward-Facing Curved Surface in Saturated Water", *Proc. 10th Int. Heat Trans. Conf.*, Brighton, England, Vol. 5, PP.45-50, August 14-18,1994.

35. El-Genk, M. S., Glebov, A. G., "Effect of Subcooling on Film Boiling from a Downward-Facing Curved Surface", *AIChE Sym. Series-Heat Transfer 306*, Vol. 91, PP. 125-131, 1995.

36. El-Genk, M. S., and Gao, C., "Pool Boiling from Downward-Facing Curved Surfaces: Effects of Radius of Curvature and Edge Angle", *Nuclear Technology*, Vol. 114, PP. 351-363, June 1996

37. Mishima, K., and Ishii, M., "Critical Heat Flux Experiments Under Low Flow Conditions in a Vertical Annulus", *NUREG/CR-2647*, 1982.

38. Cheng, L. Y. and Tichler, P. R., "Critical Heat Flux for Free Convection Boiling in Thin Rectangular Channels", *National Heat Transfer Conference*, PP. 26-31, July 1991.

39. Cheng, L. Y., "Counter-Current Flow Limited CHF in Thin Rectangular Channels", *Proc. 3rd AME-JSME Thermal Engineering Joint Conference*, ASME, 1991.

40. Fiori, M. P., and Bergles, A. E., "Model of CHF in Subcooled Boiling", Paper B 6.3, Heat Transfer 1970, Vol. 6, Proc. 4th *Int. Heat Transfer Conf.*, Versailles 1970.

41. Van der Molen, S. B., and Galjee, F., "The Boiling Mechanism During Burnout Phenomena" Proceeding of Six Int. Heat Transfer Conf. Vol. P. 381 Hemisphere Pub., Washington, D. C. 1978.

42. Ho, W.-H., Tu, K.-C., Pei, B.-S., and Chang, C.-J., "A Theoretical Critical Heat Flux Model for Low-Steam-Quality Conditions", *Nuclear Technology*, Vol. 103, PP. 332-345, Sept. 1993.

43. Katto, Y., "Prediction of Critical Heat Flux of Subcooled Flow Boiling in Round Tubes", *Int. J. Heat Mass Transfer*, Vol. 33, No. 9, PP. 1921-1928, 1990.

44. Hart, J., Ellenberger, J., and Hamersma, P. J., "Single- and Two-Phase Flow through Helically Coiled Tubes", *Chem. Eng. Sci.*, Vol. 43, PP. 775-783, 1988.

45. Weisman, J., and Pei, B. S., "Prediction of Critical Heat Flux in Flow Boiling at Low Qualities", Int. J. Heat Mass Transfer, Vol. 26, PP.1463-1477, 1983.

46. Lee, C. H., and Mudawar, "A Mechanistic Critical Heat Flux Model for Subcooled Flow Boiling Based on Local Bulk Flow Conditions", *Int. J. Multiphase Flow*, Vol. 14, PP. 711-728, 1988.

47. Ishii, M., Thermo-Fluid Dynamic Theory of Two-Phase Flow, Eyrolles, Paris, 1975.

48. Boure, J. A., "Constitutive Equations for Two-Phase Flows in Two-Phase Flows and Heat Transfer with Application to Nuclear Reactor Design Problems," Von Karman Institute Book, Hemisphere, New York, Chap. 9, 1978.

49. Carey, V. P., "Liquid-Vapor Phase-Change Phenomena", Series in Chemical and Mechanical Engineering, Taylor & Francis, 1992.

50. Hewitt, G. F., and Hall-Taylor, N. S., Annular Two-Phase Flow, Pergamon Press, Oxford, 1970.

51. Wallis, G. B., "One-Dimensional Two-Phase Flow", Wiley, New York, 1965.

52. Lockhart, R. W., and Martinelli, R. C., "Proposed Correlation of Data for Isothermal Two-Phase, Two-Component Flow In Pipes", *Chem. Eng. Prog.* Vol. 45, PP. 38-39, 1949.

53. Chisholm, D. and Laird, A. D., "Two-Phase Flow in Rough Tubes", Trans. ASME, Vol. 80, PP. 276-286, 1958.

54. Thom, J. R. S., "Prediction of Pressure Drop During Forced Circulation Boiling of Water", *Int. J. Heat Mass Transfer*, Vol. 7, PP. 709-724, 1964.

55. Barcozy, C. J., "Correlation of Liquid Fraction In Two-Phase Flow with Applications to Liquid Metals", *Chem. Eng. Prog. Symp.* Ser., Vol. 61, No. 57, PP. 179-191, 1965.

56. Zivi, S. M., "Estimation of Steady-State Steam Void-Fraction by Means of the Principle of Minimum Entropy Production", *J. Heat Transfer*, Vol. 86, PP. 247-252, 1964.

57. Martinelli, R. C., and Nelson, D. B., "Prediction of Pressure Drop During Forced-Circulation Boiling of Water", *Trans. ASME*, Vol. 70, PP. 695-702, 1948.

58. Zuber, N., "Hydrodynamic Aspects of Boiling Heat Transfer", *AEC* Rep., AECU-4439, June 1959.

59. Sadatomi, M., Sato, Y., "Two-Phase Flow in Vertical Noncircular Channels", *Int. J. Multiphase Flow*, Vol. 8, No. 6, PP. 641-655, 1982.

60. Ripple, G. R., Edit, C. M., and Jornan, H. B., "Two-Phase Flow in a Coiled Tube," I&EC, Vol. 5, PP. 32-39, 1966.

61. Owhadi, A., Bell, K. J., and Crain B., "Forced Convection Boiling Inside Helically-Coiled Tubes". *Int. J. Heat Mass Transfer*, Vol. 11, PP. 1779-1793, 1968.

62. Banerjee, S. A., and Rhodes, E., and Scott, D. S., "Studies on Concurrent

Flow in Helically Coiled Tubes, I-Flow Patterns, Pressure Drop and Holdup", *Can. J. Chem. Eng.* Vol. 47, PP. 445-453, 1969.

63. Byoce, B. E., Collier, J. G., and Levy, J., "Holdup and Pressure Drop Measurement in the Two-Phase Flow of Air-Water Mixing Tubes in Helical Coils", *Proc. of Int. Symp. on Research in Concurrent Gas and Liquid Flow*, Plenum Press, New York, PP. 203-231, 1969.

64. Akgawa, K., Sakaguchi, T., and Ueda, M., "Study on Gas-Liquid Two-Phase Flow in Helically Coiled Tubes", Bull, *JSME* Vol. 14, PP. 564-571, 1971.

65. Kasturi, G., and Stepanek, J. B. 1972a, "Two-Phase Flow-I. Pressure Drop and Void Fraction Measurement in Concurrent Gas Liquid Flow in a Coil", *Chem. Eng. Sci.*, Vol. 27, PP. 1871-1880, 1972a.

66. Dukler, A. E., Wicks, M. III, and Cleveland, R. G., "Pressure Drop and Hold-Up in Two-Phase Flow, Part A--A Comparison of Existing Correlations; and Part B--An Approach Through Similarity Analysis", *AIChE J.*, Vol. 10, PP. 38-51, 1964.

67. Kasturi, G., and Stepanek, J. B., "Two-Phase Flow-II. Parameter for Void Fraction and Pressure Drop Correlations", *Chem. Eng. Sci.*,Vol. 27, PP. 1881-1891, 1972b.

68. Rangacharyulu, K., and Davies, G. S., "Pressure Drop and Holdup Studies of Air-Liquid Flow in Helical Coils", *Chem. Eng. J.*, Vol. 29, PP. 41-46, 1984.

69. Chen, S. J., and Zhou, F. D., "An Investigation of Flow Pattern and Frictional Pressure Drop Characteristics of Air Water Two-Phase Flow in Helical Coils", *Proceeding of 4th Miami International Conference on Alternate Energy Sources*, PP. 120-129, 1981.

70. Mujawar, B. A. and Rao, M. R., "Gas Non-Newtonian Two-Phase Flow in Helical Coils", Indus. Engng Chem. Process Des. Dev., Vol. 20, PP. 391-197, 1981.

71. Hart, J., Ellenberger, J., and Hamersma, P. J., "Single- and Two-Phase Flow through Helically Coiled Tubes", Chem. Engng Sci., Vol. 43, PP. 775-783, 1988.

72. Saxena, A. K., Schumpe, A. and Nigam, K. D. P., "Flow Regimes, Holdup, and Pressure Drop for Two-Phase Flow in a Helical Coil", *Can. J. Chem. Eng.* Vol. 68, PP. 553-559, 1990.

73. Mishima, K., Ishii, M., "Flow Regime Transition Criteria for Upward Two-Phase Flow in Vertical Tubes", *Int. J. Heat Mass Transfer*, Vol. 27, No. 5, PP. 723-737, 1984.

APPENDIX B
Program Listing for Flow Calculations

```
c This main program is used to calculate the mass flow rate in the annular gap
      PROGRAM flow
      implicit none
      integer i,j
      real mass_flow,heat_input,guess_1,guess_2,mass,acc,rtbis,x(0:200)
      real theta(0:200),alpha(0:200),m,dq,jv(0:200),A(0:200)
      logical validity
      common /heat_flux/ heat_input,validity,x,theta,alpha,jv,A
      external mass
      external rtbis

      open (1, file='mass.dat', status='unknown')
      open (2, file='mass1.dat',status='unknown')
      open (3, file='mass2.dat',status='unknown')
      open (4, file='mass3.dat',status='unknown')
      read (1,*) heat_input,guess_1, guess_2,dq
      acc=1.0e-10
      do 100 i=1,10
       validity=.FALSE.
       call zbrac(mass, guess_1, guess_2, validity)
       write(6,*) guess_1, guess_2,validity
       if (.not.validity) goto 900
        mass_flow=rtbis(mass,guess_1,guess_2,acc)
        m=mass_flow
        do 55 j=0,100
          write(4,*) theta(j)*180./3.1416,x(j)*m,(1-x(j))*m,alpha(j)
     &              ,jv(j)
  55    continue
```

```
      write(2,*) mass_flow, heat_input
      write(6,*) mass_flow, heat_input
      heat_input=heat_input+dq
100   continue
      goto 999
900   write(6,*) 'there is no root in that bracket'
999   stop
      END


      REAL FUNCTION mass(m)
      implicit none
      integer i
      real c, R, z0, zp, omega, denl, denv, m, g, Cp, c1, c2, B, mv
      real Ai, zs, Pa, h, mul, muv, c3, c4, Ftp , Acce, Cg, Capm,
     &     Cai, Ca, Cg2, Cq, Ctp2, Ca2, hwi_, Dh_, flo_, alpha_,
     &     Cg3, Ctp3, L, Pi, q, Cp1,Cp2, x(0:200), theta(0:200)
      real z(0:200), alpha(0:200), A(0:200), P(0:200),jv(0:200)
      real l_(0:200), Dh(0:200), flo(0:200), Xtt(0:200),
     &     hwi(0:200), B_(0:200), D_(0:200), dg(0:200)
      logical val
      common /heat_flux/ q,val,x,theta,alpha,jv,A
c
c  assign values to some variables
      Pi=3.1416
      g=9.8
      omega=45./180.*Pi
      mv=0.1459*q/2257000.
c
c  clearance between the upper cylindrical aluminum and insulation structure
      c=0.084
```

```
      Capm=0.01905
c
c  radius of hemisphere
      R=0.1524
c
c  the column height above the bottom inlet
      L=0.5207
cc
c  the area of bottom inlet
      Ai=Pi*(1.5*0.0254)**(2.)/4.
c
c  the z-location for the theta equal to 0 degree
      z0=0.13444
      z(0)=z0
c
c  the z-location for the theta equal to 90 degree
      zp=0.28684
      z(100)=zp
c
c  the special location where the cross-sectional area changes
      zs=0.1143
c
c  the averaged pressure
      Pa=101325.
c
c  density of liquid water
      denl=957.85

c  density of water vapor
      denv=0.5956
c
```

```
c  enthalpy of evaporation
      h=2257000.
c
c  dynamic viscosity of liquid water
      mul=279.e-6
c
c  dynamic viscosity of water vapor
      muv=12.02e-6
c
c  input heat flux in this case it is assumed uniformly distributed anywhere
      B=0.4243*q
      c1=1.-(denv/denl)**(.89)*(mul/muv)**(.18)
      c2=c1/B
      c3=B*(mul/muv-1.)
      c4=B*(denl/denv-1.)
c
ccc
c
c  assign the values to z
      do 10 i=1,99,1
      z(i)=z0+i*(zp-z0)/100.
   10 continue
c
c  assign values to quality
       do 20 i=0,100,1

         x(i)=abs(B*(z(i)-z0)/m-0.00000001)
         Xtt(i)=(denv/denl)**0.5*(mul/muv)**0.125*((1.-x(i))
     &          /x(i))**0.875
c
c  assign values to void fraction
```

```
      alpha(i)=(1.+(1-x(i))/x(i)*(denv/deni)**0.67)**(-1.)
c
c  assign values to theta
      theta(i)=acos(1.-(z0-z(i))/R)
c
c  assign values to gap distance
      if (z(i) .le. 0.2159) then
       dg(i)=R*(1.-sin(theta(i))-cos(theta(i))/tan(omega))+c

c
c  assign values to cross-sectional area
       A(i)=Pi*(2.*R*dg(i)*sin(theta(i))+dg(i)**2.)*sin(omega)

c
c  assign values to perimeter
       l_(i)=2.*Pi*(2.*R*sin(theta(i))+dg(i)*sin(omega))

      else
       dg(i)=0.17145-R*sin(theta(i))
       A(i)=Pi*(0.17145**2-(R*sin(theta(i)))**2)
       l_(i)=2.*Pi*(0.17145+R*sin(theta(i)))
      endif
c
c  assign values to characteristic length
      Dh(i)=4.*A(i)/l_(i)
c
c  assign values to frictional coefficient
      flo(i)=0.316*(4.*m/mul/l_(i))**(-.25)
c
c  assign values to M-L multiplier hwi(i) note it is square!!
      hwi(i)=(1.+21./Xtt(i)+1./Xtt(i)**2)*(1-x(i))**1.75
```

```
c
c  assign values to Pressure distribution along vertical axis
       P(i)=Pa+denl*(L-z(i))*g
 20  continue
c
c  find out the integrals, first for the two-phase frictional force (Ftp)
       Do 30 i=0,100,1
         B_(i)=hwi(i)*flo(i)*2./denl/Dh(i)**2./A(i)**2./sin(omega)
 30    continue
       Ftp=0.0
       do 40 i=0,99,1
         Ftp=(z(i+1)-z(i))*(B_(i)+B_(i+1))/2.+Ftp
 40    continue
c
c  find out the integral for the acceleration term
       D_(0)=0.0
       do 50 i=1,100,1
         D_(i)=(x(i)**2./alpha(i)/denv+(1.-x(i))**2./(1.-alpha(i))
     &       /denl)/A(i)
 50    continue
       Acce=0.0
       do 60 i=0,99,1
         Acce=(1./A(i)+1./A(i+1))*(D_(i+1)-D_(i))/2.+Acce
 60    continue

c Calculate the superficial vapor velocity
       do 70 i=0,100,1
        jv(i)=m*x(i)/A(i)/denv
 70    continue
```

```
c  find out the other coefficients
c the pressure loss term due to the gradual conical expansion
      Cp=0.5*denl*(m/denl/Ai)**2.
cc
c the gravity term for whole-liquid section
      Cg=g*denl*z0
c
c the term account for the acceleration in the whole-liquid
c  section
      Cai=(1./A(0)**2.-1./Ai**2.)/2./denl*m**2


c the gravity term in the two-phase region
      Cg2=g*denl*(zp-z0)
c
c the term attributed to the change of quality
      Cq=g*(denv-denl)*((zp-z0)/c1-c2*m*log(c1*(zp-z0)+c2*m)/c1
     &     **2.+c2*m*log(c2*m)/c1**2.)
c
c the term attributed to the two-phase frictional force
c
      Ctp2=m**2.*Ftp


c
c the term attributed to the acceleration
c
      Ca2=m**2.*Acce
c
c the term account for the two-phase frictional force in upper
c  cylindrical annular gap
c
```

```
      hwi_=(1.+c3*(zp-z0)/m)**(-.25)*(1.+c4*(zp-z0)/m)
      Dh_=2.*Capm
      flo_=0.316*(2.*m/Pi/(2.*R+Capm)/mul)**(-.25)
      alpha_=(c1+c2*m/(zp-z0))**(-1.)
      A(100)=Pi*(2.*R*Capm+Capm**2.)
c
      Ctp3=m**2.*hwi_*flo_*2./denl/Dh_**2./A(100)**2.*(L-zp)
c
c the gravity term in the upper cylindrical annular gap
c
      Cg3=g*((1.-alpha_)*denl+alpha_*denv)*(L-zp)
c
c the pressure loss term due to the sudden contraction
c  at the entrance, the minor pressure is
      Cp1=0.42*0.5*denl*(m/denl/Ai)**2.

c the pressure loss due to the sudden expansion at the
c  exits.
      Cp2=1.*0.5/denl*(1.-x(100))**2.*m**2/6./(3.e-3)**2.

c  Calculated the value of mass function
c
      mass = denl*g*L-Cp-Cg -Cg2-Cq-Ctp2-Ca2-Ctp3-Cg3-Cp1-Cai
      RETURN
      END



C Subroutine: This subroutine is to find the bracket of a given pair (a,b)
    SUBROUTINE zbrac(mass, x1, x2, succes)
    INTEGER NTRY
```

```
      REAL x1,x2,mass, FACTOR
      EXTERNAL mass
      PARAMETER (FACTOR=1.005, NTRY=1000)
C
C       Given a function func and an initial guessed range x1 to x2, the
c       routine expands the range geometrically until a root is bracketed
c       by the returned values x1 and x2 (in which case sucess returns as
c       .true.) or until the range becomes unacceptably large (in which
c       case sucess returns as .false.)
c
      INTEGER j
      REAL f1, f2
      LOGICAL succes
      if (x1 .eq. x2) pause
      f1=mass(x1)
      f2=mass(x2)
      succes=.TRUE.
      do 11 j=1, NTRY
        if (f1*f2 .lt. 0.) return
        if (ABS(f1) .lt. ABS(f2)) then
          x1=x1+FACTOR*(x. -2`
          f1=mass(x1)
        else
          x2=x2+FACTOR*(x2-x1)
          f2=mass(x2)
        endif
11    continue
      succes=.FALSE.
      RETURN
      END
```

```
c
c This program is to find the root by the method of Bisection
c
      FUNCTION rtbis(mass,x1,x2,xacc)
      INTEGER JMAX
      REAL rtbis,x1,x2,xacc,mass
      EXTERNAL mass
      PARAMETER (JMAX=40)

C     Using bisection, find the root of a function func known to lie
c     between x1 and x2. The root, returned as rtbis, will be defined
c     until its accuracy is xacc.

      INTEGER j
      REAL dx,f,fmid,xmid
      fmid=mass(x2)
      f=mass(x1)
      if (f*fmid .ge. 0.) pause 'root must be bracketed in rtbis'
      if (f .lt. 0.) then
        rtbis=x1
        dx=x2-x1
      else
        rtbis=x2
        dx=x1-x2
      endif
      do 22 j=1, JMAX
        dx=dx*.5
        xmid=rtbis+dx
        fmid=mass(xmid)
        if (fmid .le. 0.) rtbis=xmid
        if (ABS(dx) .lt. xacc .or. fmid .eq. 0.) return
```

```
22  continue

    pause 'too many bisections in rtbis'

    END
```

APPENDIX C

Steady-State Nucleate Boiling Data for a Downward Facing Hemispherical Surface Surrounded by a Thermal Insulation Structure

The steady-state numerical boiling data measured at five distant spatial locations of the heated vessel surrounded by a thermal insulation structure are given in Tables C-1 to C-5. In each table, the boiling data are presented for four separate water temperatures varying from 90°C for subcooled boiling to 100°C for saturated boiling.

Table C-1: Steady State Nucleate Boiling Data at the Bottom Center With Thermal Insulation ($\theta = 0°$)

T_{sub} (°C)	T_w-T_{sat} (°C)	q''_{nb} (MW/m^2)
90	20.0020	0.4102
90	22.5106	0.5027
90	26.4978	0.6056
90	27.9526	0.6501
90	30.0124	0.7029
90	32.1005	0.7508
90	33.9724	0.8007
90	37.0621	0.8507
90	38.1144	0.9016
90	39.8985	0.9504
90	41.0023	1.0020
93	24.4970	0.4001
93	26.4897	0.5014
93	29.5102	0.6017
93	31.1001	0.6506
93	33.0111	0.7001
93	35.0012	0.7502
93	35.9986	0.8025
93	38.0123	0.8503
93	40.1003	0.9011
93	41.0571	0.9505
93	42.0687	1.0100
97	28.5012	0.4020
97	33.0134	0.5111
97	36.5025	0.6058
97	38.3101	0.6509
97	40.5106	0.7108
97	42.8042	0.7509

97	44.8053	0.8012
97	47.0587	0.8512
97	48.1002	0.9112
97	49.1030	0.9507
97	50.0284	1.0010
100	30.1012	0.4008
100	34.0225	0.5016
100	38.0558	0.6102
100	40.1011	0.6511
100	42.2106	0.7120
100	44.0254	0.7505
100	46.1089	0.8115
100	48.5157	0.8501
100	50.5158	0.9177
100	52.1144	0.9524
100	53.5088	1.0120

Table C-2: Steady State Nucleate Boiling Data at an Off-Center Location with Thermal Insulation ($\theta = 18°$)

T_{sub} (°C)	T_w-T_{sat} (°C)	q''_{nb} (MW/m^2)
90	13.0520	0.4013
90	15.0726	0.5055
90	17.0877	0.5975
90	18.1006	0.6498
90	20.0102	0.7102
90	21.4978	0.7511
90	22.4935	0.8133
90	23.4965	0.8520
90	24.5033	0.8983
90	25.4963	0.9536
90	26.5047	1.0120
93	16.0112	0.4007
93	18.0252	0.5036
93	20.0774	0.6087
93	22.1000	0.6490
93	23.9702	0.7105
93	24.2945	0.7511
93	24.5044	0.8235
93	25.5028	0.8514
93	26.5011	0.9058
93	27.4957	0.9535
93	28.5043	1.0240
97	21.0140	0.4052
97	25.0354	0.5065
97	28.0014	0.6087
97	31.0071	0.6527
97	33.1002	0.7060
97	34.9756	0.7563
97	36.9857	0.8075

97	39.0453	0.8542
97	41.5010	0.9053
97	44.0245	0.9532
97	45.0557	1.0460
100	21.5004	0.4053
100	26.0782	0.4985
100	28.9623	0.6075
100	31.5014	0.6531
100	33.4953	0.7134
100	36.0775	0.7552
100	37.9573	0.8024
100	40.0112	0.8503
100	42.0021	0.9025
100	43.0568	0.9563
100	44.0412	1.0320

Table C-3: Steady-State Nucleate Boiling at an Off-Center Location with Thermal Insulation ($\theta = 45°$)

Tsub (oC)	Tw-Tsat (oC)	q"nb (MW/m2)
90	7.6085	0.4019
90	9.8075	0.5067
90	11.2871	0.5530
90	12.7779	0.6030
90	14.2109	0.6538
90	15.7243	0.7122
90	17.4879	0.7485
90	19.0639	0.8013
90	21.0608	0.8509
90	21.7297	0.9071
90	33.0175	0.9539
93	8.3882	0.4052
93	10.5865	0.5085
93	11.7981	0.5519
93	13.3043	0.5963
93	14.5861	0.6505
93	16.2080	0.7063
93	17.9111	0.7512
93	20.3020	0.8048
93	22.1058	0.8524
93	23.065	0.9032
93	28.3083	0.9504
97	10.2363	0.4047
97	13.5063	0.5018
97	15.1120	0.5514
97	16.5987	0.6021
97	18.5264	0.6529
97	19.7271	0.7094
97	22.1091	0.7535

97	24.2032	0.8054
97	25.9042	0.8512
97	24.7065	0.8527
97	26.8053	0.9055
97	30.1854	0.9507
97	34.0528	1.0260
100	8.8845	0.4007
100	12.1133	0.5068
100	14.0204	0.5518
100	15.7976	0.6019
100	17.0668	0.6536
100	20.0189	0.7084
100	21.5249	0.7524
100	24.6077	0.8013
100	27.4036	0.8506
100	30.1076	0.9010
100	33.5086	0.9516
100	37.0790	1.0070

Table C-4: Steady State Nucleate Boiling Data at an Off-Center Location with Thermal Insulation ($\theta = 60°$)

T_{sub} (°C)	T_w-T_{sat} (°C)	q''_{nb} (MW/m^2)
90	7.4197	0.4028
90	9.7061	0.5059
90	11.0083	0.5518
90	12.5159	0.6042
90	14.0193	0.6507
90	15.0663	0.7053
90	16.6123	0.751
90	17.9228	0.8178
90	19.9199	0.8524
90	20.042	0.9064
90	23.0458	0.9514
93	7.5071	0.4078
93	9.0672	0.5045
93	11.2836	0.5519
93	12.7965	0.6064
93	14.0239	0.6525
93	15.8015	0.7089
93	17.2136	0.7516
93	18.9001	0.8020
93	21.0627	0.8524
93	22.4938	0.9088
93	24.6053	0.9520
93	27.0783	1.0480
97	9.2076	0.4046
97	12.5046	0.5064
97	14.2035	0.5512
97	15.8086	0.6067
97	17.6054	0.6513
97	19.0991	0.7080

97	21.7176	0.7508
97	23.9259	0.8074
97	28.4463	0.9017
97	31.4379	0.9521
97	45.4295	1.002
100	11.0782	0.4025
100	15.0375	0.5042
100	17.083	0.5517
100	19.7198	0.6072
100	22.3086	0.6542
100	23.7128	0.7057
100	25.6885	0.7515
100	29.1961	0.7991
100	31.7218	0.8534
100	34.5065	0.9009
100	38.8972	0.9501
100	55.1011	1.0450

Table C-5: Steady State Nucleate Boiling Data at an Off-Center Location with Thermal Insulation ($\theta = 75°$)

T_{sub} (°C)	T_w-T_{sat} (°C)	q''_{nb} (MW/m^2)
90	7.2010	0.4023
90	9.5052	0.5074
90	10.8960	0.5514
90	12.5062	0.6013
90	13.8725	0.6527
90	15.4861	0.7118
90	17.0526	0.7529
90	18.2077	0.8102
90	20.2854	0.8532
90	21.5015	0.9088
90	23.7014	0.9510
93	7.3041	0.4054
93	10.0972	0.5063
93	11.0374	0.5510
93	12.4032	0.5967
93	13.7783	0.6486
93	15.2085	0.6958
93	16.7047	0.7485
93	18.5065	0.8002
93	20.2016	0.8511
93	21.6872	0.9005
93	22.9021	0.9503
93	24.5033	1.0110
97	8.5942	0.4033
97	11.9011	0.5057
97	13.2831	0.5511
97	15.1076	0.6096
97	17.0273	0.6487
97	17.8761	0.7006

97	20.3046	0.7518
97	21.9035	0.8085
97	22.7023	0.8509
97	24.6025	0.9025
97	27.2952	0.9506
97	30.0026	1.0220
100	8.9001	0.4026
100	12.1025	0.5013
100	14.0457	0.5493
100	15.0865	0.6020
100	16.7010	0.6525
100	19.1877	0.7059
100	20.8955	0.7534
100	24.0125	0.8094
100	26.7901	0.8502
100	29.1133	0.9032
100	31.5136	0.9501
100	33.5126	1.0450

NRC FORM 335 (2-89) NRCM 1102, 3201, 3202

U.S. NUCLEAR REGULATORY COMMISSION

BIBLIOGRAPHIC DATA SHEET

(See instructions on the reverse)

1. REPORT NUMBER (Assigned by NRC, Add Vol., Supp., Rev., and Addendum Numbers, if any.)

NUREG/CR-5534
PSU/ME-98-7321

2. TITLE AND SUBTITLE

Critical Heat Flux (CHF) Phenomenon on a Downward Facing Curved Surface: Effects of Thermal Insulation

3. DATE REPORT PUBLISHED

MONTH: September YEAR: 1998

4. FIN OR GRANT NUMBER

J6030

5. AUTHOR(S)

F. B. Cheung and Y. C. Liu

6. TYPE OF REPORT

TECHNICAL

7. PERIOD COVERED (Inclusive Dates)

7/7/93 to 7/6/98

8. PERFORMING ORGANIZATION – NAME AND ADDRESS (If NRC, provide Division, Office or Region, U.S. Nuclear Regulatory Commission, and mailing address; if contractor, provide name and mailing address.)

Department of Mechanical Engineering
The Pennsylvania State University
University Park, PA 16803

9. SPONSORING ORGANIZATION – NAME AND ADDRESS (If NRC, type "Same as above", if contractor, provide NRC Division, Office or Region, U.S. Nuclear Regulatory Commission, and mailing address.)

Division of Systems Technology
Office of Nuclear Regulatory Research
U.S. Nuclear Regulatory Commission
Washington, D.C. 20555-0001

10. SUPPLEMENTARY NOTES

A. Behbahani, NRC Project Manager

11. ABSTRACT (200 words or less)

The phenomena of natural convection boiling and critical heat flux on the outer surface of a heated hemispherical vessel surrounded by a thermal insulation structure were investigated experimentally in the subscale boundary layer boiling (SBLB) test facility. The objectives were to measure the rate of boiling heat transfer, to observe the behavior of the boiling-induced two-phase motion in the annular channel between the hemispherical vessel and the insulation structure, and to determine the flow effect on the critical heat flux on the downward-facing hemispherical surface. High-speed photographic records revealed the presence of violent cyclic ejection of the vapor masses generated by boiling on the vessel outer surface which resulted in a buoyancy-driven, upward, co-current two-phase flow through the channel. A one-dimensional analysis of the co-current flow in the channel indicated that the induced mass flow rate was a strong function of the wall heat flux and the size of the channel. Measurements of the local boiling heat fluxes and the local wall superheats showed a significant spatial variation of the nucleate boiling heat transfer, evidently due to the effect of the upward co-current flow. At high heat flux levels, the steam venting process through the minimum gap of the channel was found to be highly unsteady and chaotic. Owing to the chaotic steam venting process, the local critical heat flux had the lowest value near the minimum gap. However, this lowest value is still higher than the corresponding local CHF value for the case without thermal insulation.

12. KEY WORDS/DESCRIPTORS (List words or phrases that will assist researchers in locating the report.)

Critical Heat Flux
Natural Convection Boiling
Thermal Insulation Structure
Lower Head Integrity
In-Vessel Retention

13. AVAILABILITY STATEMENT

Unlimited

14. SECURITY CLASSIFICATION

(This Page) Unclassified

(This Report) Unclassified

15. NUMBER OF PAGES

16. PRICE

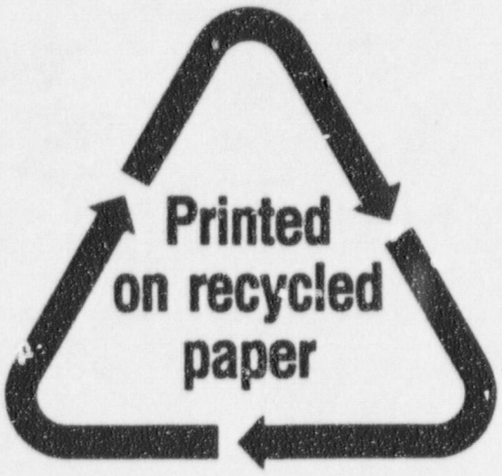

Federal Recycling Program